[American Journal of Science, Vol. 314, February, 2014, P. 679–703, DOI 10.2475/02.2014.08]

GEOCHRONOLOGIC AND GEOCHEMICAL EVIDENCE FOR PERSISTENCE OF SOUTH-DIPPING SUBDUCTION TO LATE PERMIAN TIME, LANGSHAN AREA, INNER MONGOLIA (CHINA): SIGNIFICANCE FOR TERMINATION OF ACCRETIONARY OROGENESIS IN THE SOUTHERN ALTAIDS

LI'NA LIN*,**, WENJIAO XIAO***,†, BO WAN***,§, BRIAN F. WINDLEY§§, SONGJIAN AO*, CHUNMING HAN*,***, JIANYUN FENG*,**, JI'EN ZHANG*, and ZHIYONG ZHANG*

ABSTRACT. The Langshan area in Inner Mongolia is situated in the southern Altaids between the Beishan suture to the west and the Solonker suture to the east. This paper addresses the poorly known tectonic evolution that led to formation of the terminal Solonker suture. Dating of deformed porphyries and undeformed dolerites and gabbros constrains the timing of the relevant NE-E-striking and north-vergent deformation. Deformed granitic-granodioritic porphyries in this area are characterized by high SiO_2 (65.38-78.00%), low TFe_2O_3 (1.29-5.07%), MgO (0.13-0.63%), and variable K_2O (0.53-4.14%) and Na_2O (2.05-4.62%). All samples have enriched LREE (La/Yb 6-18) and negative Nb anomalies (Nb_N/Th_N0.09-0.48), but different Eu anomalies (Eu* <0.7 or ~1); these geochemical features can be ascribed to a heterogeneous source in a subduction-related environment. Gabbros and dolerites have 42.33 to 52.03 percent SiO_2. All mafic samples have similar La/Yb ratios of 4 to 6 and negative Nb anomalies (Nb_N/Th_N) ratios of 0.2 to 0.8, suggestive of a subduction-related setting. Two granitic porphyries yielded $^{238}U/^{206}Pb$ weighted mean ages of 284.7 ± 2.1 Ma with MSWD of 1.6 and 291.7 ± 2.1 Ma with MSWD of 1.14; these ages are consistent with $^{235}U/^{207}Pb$ and $^{238}U/^{206}Pb$ concordia ages of 281 ± 17 Ma with MSWD of 0.87 and 289.8 ± 9.2 Ma with MSWD of 0.66. A dolerite yielded concordia ages of 256.2 ± 2.6 Ma with MSWD of 0.44 and 256 ± 2.5 Ma with MSWD 0.45. The ages and geochemistry of the deformed porphyries indicate that in the early Permian there was important deformation and recrystallization in a subduction-related setting. The isotopic and geochemical signatures of all the rocks indicate that they formed during subduction-related conditions. We propose that Langshan was a Permian active continental margin arc built on the edge of the North China Craton by southward subduction, which led to closure of the ocean, concomitant formation of the Solonker suture in the late Permian-early Triassic, and termination of the accretion-subduction orogen of the southern Altaids.

Key words: Langshan, Permian, accretionary tectonics, North China Craton, Andean-type arc

INTRODUCTION

The Central Asian Orogenic Belt (CAOB) or its younger half, the Altaids (Sengör and others, 1993; Jahn and others, 2004; Wilhem and others, 2012) extends from the Urals through Kazakhstan, northern China, Mongolia and southern Siberia to the Okhotsk Sea in the Russian Far East—the largest accretionary collage on the planet (fig. 1 inset). The evolution of this huge orogenic collage between the Baltic, Siberia, Tarim and North China Cratons was related to the closure of the Paleo-Asian Ocean (Zonenshain and others, 1990; Sengör and others, 1993; Jahn and others, 2004;

* State Key Laboratory of Lithospheric Evolution, Institute of Geology and Geophysics, Chinese Academy of Sciences, Beijing 100029, China
** Graduate University of Chinese Academy of Sciences, Beijing 100049, China
*** Xinjiang Research Center for Mineral Resources, Xinjiang Institute of Ecology and Geography, Chinese Academy of Sciences, Urumqi 830011, China
§ Department of Geological Sciences, Stockholm University, Stockholm 106 91, Sweden
§§ Department of Geology, University of Leicester, Leicester, LE1 7RH, UK
† Corresponding author: wj-xiao@mail.igcas.ac.cn; Tel: +86-10-8299-8524; Fax: +86-10-6201-0846

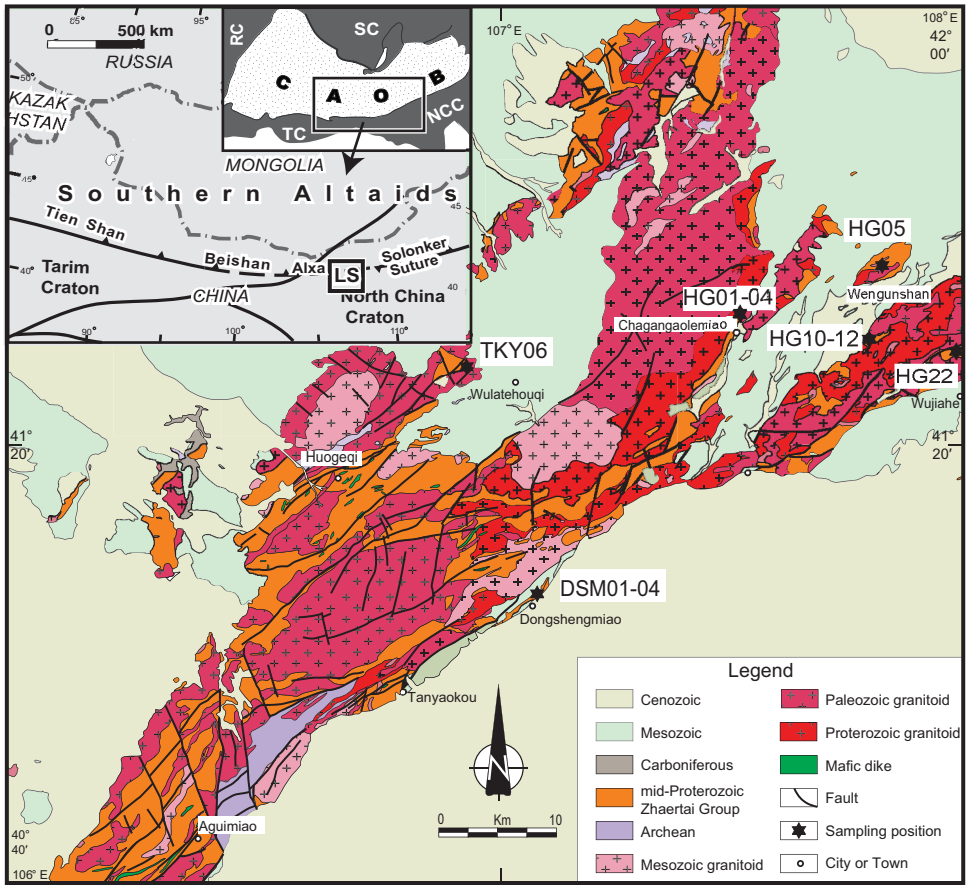

Fig. 1. Simplified map of the main geology of the Langshan region showing the location of our analyzed samples (after Anonymous, 1980, 1981). Inset map shows the position in Inner Mongolia (after Xiao and others, 2009). RC-Russia Craton, SC-Siberia Craton, TC-Tarim Craton, NCC-North China Craton, LS-Langshan.

Kröner and others, 2007; Windley and others, 2007; Xiao and others, 2013). Since the benchmark paper by Sengör and others (1993), extensive studies have been conducted in this orogen, which made considerable progress in understanding its evolution (for example, Allen and others, 1993; Cunningham and others, 1996; Sengör and Natal'in, 1996; Badarch and others, 2002; Windley and others, 2002; Xiao and others, 2003, 2010a; Alekseev and others, 2007; Charvet and others, 2007). Although it was earlier considered that the whole collage evolved from a single arc (Sengör and others, 1993; Sengör and Natal'in, 1996), it is now most widely accepted that it developed as an archipelago (Coleman, 1989; Hsü and others, 1991; Hsü, 2003; Xiao and others, 2009), largely as a result of progressive accretion of material onto the southern edge of the Siberian Craton (present coordinate). Evidence for the early stage of this orogen is provided by a *ca.* 1.0 Ga ophiolite in the northern Altaids close to the Siberian southern margin (Khain and others, 2002). However, there are different opinions about the timing and the types of final stages that led to termination of the orogenic collage: for example in the Carboniferous (Dobretsov and others, 1995; Zhang, S. H. and others, 2009) or in the Permian (Tang, 1990; Chen and others, 2000, 2009; Xiao and others, 2003; Jian and others, 2010).

In general, establishing the timing of orogenic events is a persistent geological problem worldwide, and no single method can directly tell us precisely when an orogenic event terminates (Sengör, 1991). One of the best constraints on the earliest stage of a plate tectonic cycle is oceanic plate stratigraphy (see for example Kusky and others, 2013), and constraints on the latest stages include post-orogenic granites (see for example, Chen and others, 2009). Extensive regional metamorphism takes place during the peak of orogenesis and is easily dateable in high-grade rocks, and high/ultrahigh pressure (HP/UHP) rocks can usefully document the time and amount of deepest subduction (see for example, Gao, 1997). Large-scale deformation and regional metamorphism was caused either by subduction or collision (see for example, Dewey, 1969).

The Langshan (Wolf Mountain in Chinese) area in Inner Mongolia is situated between the Beishan and Solonker sutures (fig. 1). Because of the presence of extensive Precambrian rocks, it has long been considered as the northern margin of the North China Craton (Zhao and others, 2001; Zhai and Liu, 2003; Darby and Ritts, 2007; Zhang and others, 2013), and also it was interpreted by Lu and others (2002) as the "Langshan rift system." Moreover, many large strata-bound Proterozoic, base metal deposits (Zhaertai Group) in the Langshan area are probably syn-sedimentary in origin (see for example, Ding and Jiang, 2000; Peng and Zhai, 2004; Li and others, 2007; Peng and others, 2007, 2010). Because of the scarcity of Paleozoic strata, the Paleozoic history of the Langshan area has been poorly studied; early characterizations of this region as part of a stable craton (Zhai and Liu, 2003) or "Proterozoic rift" (Lu and others, 2002) are incompatible with the currently known geology. In addition, it is still not known whether the considerable deformation in the area was caused by the 1.85 Ga collision between the West and East North China blocks (Zhao and others, 2001) or by other younger tectonic events. Constraining the time of deformation in Langshan is the key to resolve the current problems. Understanding the Langshan geology in a regional context will greatly improve our knowledge of the southern Altaids and the Paleozoic history of this part of North China.

In the field we collected samples of intrusive rocks that were deformed together with Proterozoic sediments and undeformed mafic dikes in order to analyze their geochemical composition and isotopic age. The aims of this study are: (a) to use the geochemical characteristics of these deformed intrusions to infer their petrogenetic settings; (b) to obtain the emplacement age of the intrusions and constrain the minimum age of their deformation; (c) to discuss and rationalize the controversial issue of the time of termination of the orogen; (d) to shed light on the regional distribution of the southern Altaids.

GEOLOGICAL BACKGROUND AND SAMPLING

The Altaids evolved over a long time-period when it made a huge contribution to our understanding of the crustal growth of Central Asia (Sengör and others, 1993; Kröner and others, 2014). Regional variations make it difficult to summarize the tectonic history of the orogen, but see Xiao and others (2003) and Feng and others (2013).

The Langshan area is bound by the Gobi desert to the NW and Cenozoic sediments to the SW (fig. 1). Prominent are extensive, but poorly studied, granitic rocks; limited isotopic ages suggested that most formed in the Paleozoic and Mesozoic and some in the Proterozoic (Anonymous, 1980).

In the south-west high-grade Archean rocks comprise amphibolites and schistose to migmatitic gneisses, which are overlain unconformably by Proterozoic metasediments (Anonymous, 1981); these Archean and Proterozoic rocks were considered to be part of the North China Craton (Zhao and others, 2001). The Proterozoic,

sedimentary >3000 m-thick Zhaertai Group comprises shale, sandstone and carbonate, and local volcanic interbeds, now seen as schist, quartzite, marble and amphibolite (Anonymous, 1981). The Zhaertai Group underwent greenschist to amphibolite facies metamorphism during deformation (figs. 2A and 2B). Because of their thick sandstones and carbonates, the Zhaertai sedimentary association was interpreted as a rift, namely the "Langshan rift system" (see for example, Lu and others, 2002); the deposition and deformation ages of the Zhaertai Group sediments are poorly constrained, but mainly interpreted as Precambrian. A mid-Proterozoic age for the Zhaertai Group was first proposed by Anonymous (1981) on the basis of stromatolites by comparison with other places. A subsequent U-Pb zircon age of *ca.* 1.75 Ga was obtained from an amphibolite interbedded with sedimentary rocks (Li and others, 2007). More recently, a meta-rhyolite has yielded a U-Pb zircon age of *ca.* 810 Ma (Peng and others, 2010). The Proterozoic Zhaertai Group is unconformably overlain by late Paleozoic volcanic and sediment rocks—in the western Langshan area. Undeformed Mesozoic conglomerates overlie the older rocks (figs. 2C and 2D).

In the SE and NW of the area the main deformation produced a train of regional, open to tight synclines with minor intraformational "Z" and "S" folds, and an associated penetrative axial plane cleavage (S_1). In pelitic rocks, S_1 is a low-grade greenschist facies slaty cleavage composed of quartz + chlorite + plagioclase + white mica, whereas sandstones show a coarsely spaced, quartzose cleavage.

Minor folds are asymmetric, tight to isoclinal, verge to the SE, their wavelengths are up to 0.5 to 3 m, their axial surfaces dip to the NW (fig. 3A), and crenulation fold axes and associated bedding-cleavage intersection lineations trend NE-SW and plunge variably to the NE or SW (fig. 3B).

The study area contains a complex network of dominant thrusts and sub-vertical strike-slip faults, well visible on aerial photographs and satellite images. Predominant are NE/SW-trending thrusts and NNE/SSW- or NNW/SSE-trending strike-slip faults mostly with sinistral displacements; later strike-slip faults consistently cut the main thrusts.

Seventeen samples of intrusive rocks were collected in 5 localities (fig. 1) from the Zhaertai Group (DSM 04-A, B, C); three samples were collected from the Lower Zhaertai Group in the northeast of the Dongshenmiao area (figs. 2E and 2F). HG 01A, B (figs. 2G and 2H) and HG 03 A, B four samples were from the Upper Zhaertai Group in the Chaganguolemiao area. HG05 A, B two samples from the Wenguanshan area also occurred in the Upper Zhaertai Group. HG 22 A, B and HG 23 A, B sampled at Wujiahe in the Upper Zhaertai Group. All samples have undergone deformation and low-grade metamorphism. For example, the light-colored intrusions, shown in figure 2E, were emplaced as sills sub-parallel to bedding and were later folded together with the sediments; the texture is porphyritic and pyroclastic (fig. 2F). Figure 2G shows an intrusive contact between meta-sediments and felsic porphyry, which contains quartz, feldspar, biotite and chlorite, indicative of greenschist facies metamorphism (fig. 2H). Figures 2F and 2H show that biotite and chlorite wrap around a rotated plagioclase porphyroclast, as a result of deformation. In contrast, the wall rocks have undergone amphibolite facies metamorphism characterized by interlayered plagioclase and hornblende plus magnetite (fig. 2B). TYK06 is from a gabbro dike near the Huogeqi area (fig. 2H), which is vertical, has a variable width (40 cm-2 m) and shows no effects of deformation. HG04, HG08 are gabbro dikes and HG11 is a doleritic dike, all collected from the Wenguanshan area; these mafic rocks are hardly metamorphosed and show no later metamorphic overprint (fig. 2J). We studied the geochemistry of all samples and the geochronology of DSM04, HG11 and HG22; the methods and results are described in the following section.

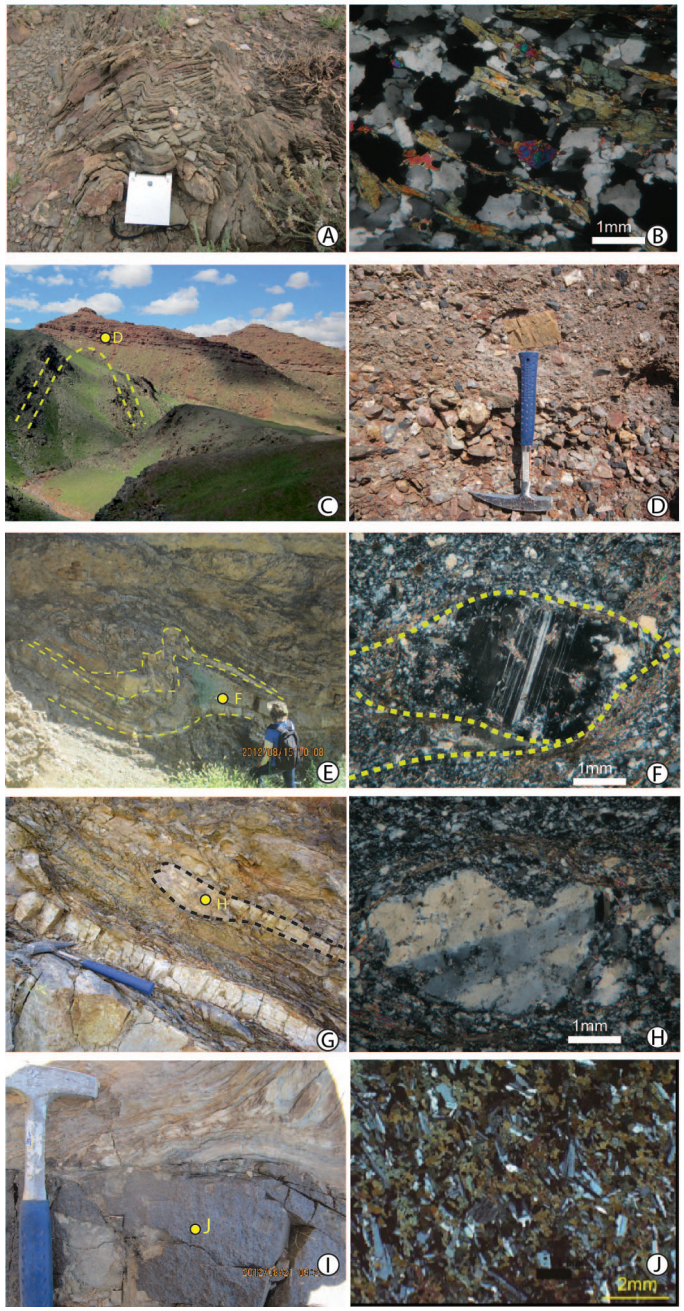

Fig. 2. Field photographs and microphotographs of key structures and lithologies. (A) Deformed amphibolite in the Zhaertai Group. (B) Preferred orientation of amphibole and feldspar defining the foliation of amphibolite. (C) Mesozoic conglomerate unconformably overlying (point d) folded Proterozoic Zhaertai Group sediments. (D) Mesozoic conglomerate with granitic, volcanic and sedimentary pebbles. (E) Conformable Mesozoic sills of porphyry in Proterozoic sediments, later folded together. (F) Porphyritic texture of a porphyry intrusion showing a cataclastic rotated feldspar porphyroclast. (G) Intrusive relationship between a Mesozoic porphyry sill and sediments of the Upper Zhaertai Group. (H) Deformed quartz porphyroclast in a feldspar + quartz matrix in a porphyry. (I) Mesozoic gabbro dike (dark) intruded in Proterozoic Zhaertai Group sediments (light) with dextral shear. (J) Unaltered ophitic texture of pyroxene and plagioclase in a gabbro dike.

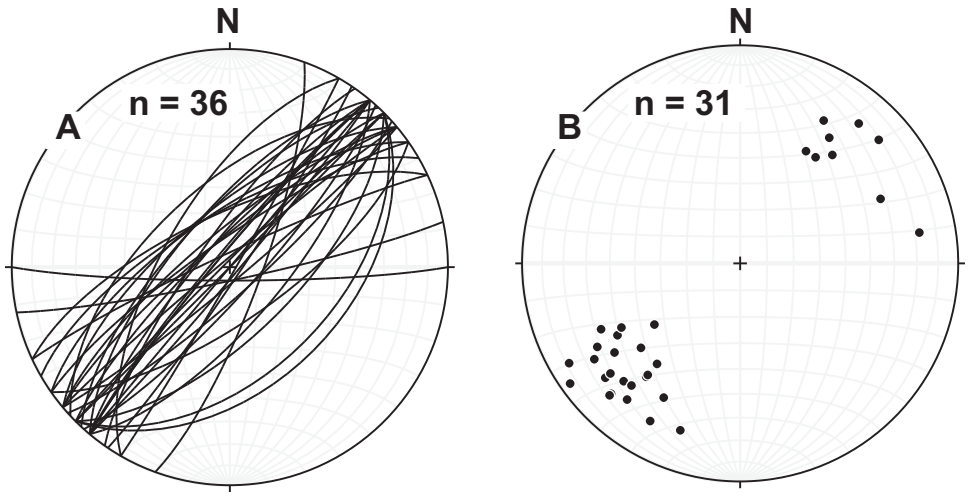

Fig. 3. (A) Stereographic projection showing the predominant regional NE-SW orientation of fold axial surfaces, (B) Stereographic projection illustrating the regional trend and plunge of fold axes. Plots are equal-angle; n is number of plotted data.

ANALYTICAL METHODS AND RESULTS

Analytical Methods

Rock chips were ground in an agate mill, and prepared for whole-rock sample analysis. Zircons were separated by a combination of heavy liquid and magnetic techniques, then mounted in epoxy resin and polished to remove the upper one third of the grains. Cathodoluminescence (CL) images were obtained in order to identify internal structures and choose potential target sites for U-Pb analyses.

Whole-rock geochemistry.—Major element oxides were analyzed on fused glass disks employing a Phillips PW 1500 X-ray fluorescence spectrometer. The precision and accuracy of the major-element data that were determined with the Chinese whole-rock granite standard GSR-1 are ≤5 percent and *ca.* 5 percent (2σ), respectively. The chemical analyses were carried out at the Institute of Geology and Geophysics, Chinese Academy of Sciences (IGGCAS), and all results are listed in table 1.

Trace element abundances were determined by ICP-MS (VG-PQII) at the IGGCAS. The sample powders were decomposed in a mixture of distilled HF-HNO_3 in Savillex Teflon® beakers for 6 days at 120 °C. The sample solution was dried and the residue dissolved in 50 ml 1 percent HNO_3 for ICP-MS analysis. Indium was used as an internal standard for correction of matrix effects and instrumental drift. The procedural blank contribution for the trace elements in table 1 is ≤446 pg and not significant considering the high concentrations of incompatible elements in the granitoids. The precision and accuracy of the data are better than 5 percent as determined on GSR-1, and all the results are presented in table 1.

Ion microprobe for U-Pb isotopes.—Measurements of U, Th, and Pb isotopes of zircon were conducted using a Cameca-IMS 1280 large-radius SIMS at IGGCAS. Zircon U-Th-Pb ratios and absolute abundances were determined relative to the standard zircon 91500 (Wiedenbeck and others, 1995 analyses of which were interspersed with those of unknown grains, using operating and data processing procedures similar to those described by Li, X. and others (2009). A long-term uncertainty of 1.5 percent (1 RSD) for $^{206}Pb/^{238}U$ measurements of the standard zircons was propagated, despite

Table 1

Major and trace element contents of whole-rock samples

	DSM04A	DSM04B	DSM04C	HG01A	HG01B	HG03A
N	41°05'48''	41°05'47''	41°05'48''	41°30'49.4''	41°30'49.3''	41°30'3.6''
E	107°02'59''	107°03'1.6''	107°02'59.3''	107°28'21.1''	107°28'21''	107°28'25.3''
SiO_2 wt.%	74.53	75.07	74.3	78	75.94	66.31
TiO_2	0.1	0.1	0.11	0.05	0.06	0.54
Al_2O_3	13.52	13.64	13.35	12.32	13.35	15.33
Fe_2O_3T	1.35	1.29	1.38	0.36	0.63	3.92
MnO	0.02	0.01	0.02	0.04	0.01	0.04
MgO	0.61	0.39	0.61	0.13	0.14	1.92
CaO	1.33	0.89	1.58	0.66	0.52	1.48
Na_2O	6.29	6.49	5.73	3.42	4.01	4.43
K_2O	0.54	0.53	0.82	3.85	3.91	4.14
P_2O_5	0.06	0.09	0.06	0.02	0.06	0.3
LOI	1.38	0.78	1.86	0.62	0.68	1.58
Total	99.73	99.28	99.82	99.47	99.31	99.99
Cs ppm	0.10	0.08	0.11	15.86	12.78	6.62
Rb	8.35	1.84	11.03	151	112	101
Ba	688	654	1022	1021	1137	1376
Th	2.68	1.80	2.58	3.03	1.65	10.9
U	0.46	0.40	0.43	0.63	0.64	0.75
Nb	7.71	7.22	7.30	10.98	4.41	9.24
Ta	0.57	0.55	0.56	0.83	0.46	0.43
La	9.32	5.70	3.91	3.3	3.8	58.1
Ce	18.3	10.8	7.00	5.59	4.54	117
Pb	3.21	2.26	2.64	17	34	14
Pr	1.81	1.22	0.77	0.79	0.75	12.43
Sr	145	95	120	106	102	371
Nd	6.22	4.18	2.59	2.72	2.60	42
Zr	86	92	85	56	60	336
Hf	2.62	2.71	2.60	2.21	2.32	8.54
Sm	0.95	0.62	0.40	0.48	0.51	5.47
Eu	0.31	0.22	0.05	0.06	0.06	0.92
Gd	0.84	0.56	0.37	0.32	0.45	4.09
Tb	0.13	0.08	0.06	0.05	0.08	0.47
Dy	0.81	0.54	0.45	0.36	0.46	2.12
Y	5.36	3.61	3.63	2.72	2.97	10.5
Ho	0.19	0.13	0.12	0.09	0.10	0.41
Er	0.61	0.43	0.43	0.30	0.26	1.13
Tm	0.10	0.08	0.08	0.05	0.04	0.17
Yb	0.78	0.63	0.63	0.36	0.27	1.11
Lu	0.14	0.11	0.12	0.06	0.04	0.17
La/Yb	12	9	6	9	14	53
Nb_N/Th_N	0.34	0.48	0.34	0.43	0.32	0.10
Eu*	1.0	1.1	0.4	0.5	0.4	0.6
Σ REE	40	25	17	14	14	245

the fact that the measured $^{206}Pb/^{238}U$ error in a specific session is generally around 1 percent (1 RSD) or less (Li, Q. and others, 2010). Measured compositions were corrected for common Pb using non-radiogenic ^{204}Pb. Corrections are sufficiently small to be insensitive to the choice of common Pb composition, and an average of

Table 1
(continued)

	HG03B	HG05A	HG05B	HG22A	HG22B	HG23A
N	41°30'3.7''	41°30'10.2''	41°30'16.4''	41°45'25''	41°45'26''	41°45'26''
E	107°28'25.2''	107°28'32''	107°28'33''	108°2'45''	108°2'44''	108°02'45''
SiO_2 wt.%	65.38	77.72	73.94	75.96	75.9	73.7
TiO_2	0.71	0.08	0.13	0.13	0.13	0.17
Al_2O_3	14.9	11.84	13.15	14.25	14.11	13.9
Fe_2O_3T	5.07	1.71	3.71	0.76	0.80	1.74
MnO	0.04	0.03	0.04	0.01	0.01	0.02
MgO	1.8	0.31	0.63	0.26	0.23	0.26
CaO	1.47	0.62	1.02	0.81	0.69	1.1
Na_2O	4.72	2.97	2.05	3.99	3.81	4.72
K_2O	3.36	3.36	2.79	3.02	3.2	3.2
P_2O_5	0.44	0.06	0.04	0.03	0.03	0.03
LOI	1.88	0.76	1.34	1.06	1.1	0.92
Total	99.77	99.46	98.84	100	100	99.76
Cs ppm	3.72	2.31	2.26	1.79	2.65	1.30
Rb	99	120	103	67	75	78
Ba	1085	440	387	641	817	1213
Th	8.76	19.7	19.9	13.2	12.8	11.2
U	1.06	2.05	1.61	4.08	4.10	2.92
Nb	9.29	6.32	4.75	6.87	7.13	8.35
Ta	0.43	1.03	0.60	0.66	0.68	0.62
La	72.1	30.7	23.5	27.6	28.4	45.5
Ce	138	56	44	49	48	89
Pb	18	20	16	15	15	50
Pr	14.54	6.21	4.84	5.24	5.27	10.13
Sr	406	124	109	165	183	300
Nd	46	21	17.0	19.1	18.0	37
Zr	349	66	73	145	148	208
Hf	8.85	2.40	2.60	4.32	4.39	6.14
Sm	6.36	3.72	3.02	3.10	2.99	6.04
Eu	1.30	0.41	0.34	0.60	0.63	0.81
Gd	4.68	2.41	2.12	2.63	2.55	4.98
Tb	0.51	0.32	0.32	0.39	0.38	0.72
Dy	2.24	1.57	1.77	2.19	2.17	4.13
Y	11.7	7.20	9.58	11.91	12.00	21.3
Ho	0.44	0.29	0.33	0.46	0.47	0.85
Er	1.15	0.73	0.89	1.32	1.31	2.40
Tm	0.17	0.10	0.13	0.20	0.20	0.37
Yb	1.05	0.68	0.83	1.43	1.38	2.48
Lu	0.16	0.10	0.13	0.24	0.23	0.38
La/Yb	69	45	28	19	21	18
Nb_N/Th_N	0.13	0.04	0.03	0.06	0.07	0.09
Eu*	0.7	0.4	0.4	0.6	0.7	0.5
ΣREE	289	125	99	113	112	204

present-day crustal composition (Stacey and Kramers, 1975) was used for the common Pb assuming that the common Pb is largely surface contamination introduced during sample preparation. Uncertainties of individual analyses in data tables are reported at

TABLE 1
(continued)

	HG23B	HG04	HG08	HG11	TYK06
N	41°45'26''	41°30'11''	41°35'45''	41°30'50''	41°26'0''
E	108°02'44.6''	107°28'32''	107°47'19''	107°45'22''	106°55'50''
SiO_2 wt.%	73.56	50.91	47.4	42.33	52.03
TiO_2	0.18	1.4	1.33	1.93	1.36
Al_2O_3	14.22	12.79	13.41	11.81	16.94
Fe_2O_3T	1.15	12.47	15.15	17.99	8.19
MnO	0.02	0.18	0.2	0.2	0.12
MgO	0.23	5.84	7.81	9.61	6.31
CaO	1.16	7.05	8.98	12.81	7.46
Na_2O	4.26	0.67	2.65	1.11	3.73
K_2O	4.18	4.64	1.42	0.22	1.5
P_2O_5	0.03	0.14	0.15	0.07	0.17
LOI	0.92	3.42	1.02	0.88	2.12
Total	99.91	99.51	99.52	98.96	99.93
Cs ppm	1.59	20.17	2.39	0.11	4.85
Rb	100	255	54	2.68	66
Ba	1344	316	480	135	287
Th	11.0	1.60	0.94	0.18	3.0
U	2.73	1.25	0.21	0.11	0.82
Nb	8.67	6.79	4.99	1.18	4.59
Ta	0.63	0.54	0.34	0.05	0.36
La	44.7	9.62	11.01	4.71	12.3
Ce	87	19.9	23	12.2	27
Pb	13.33	25	8.75	1.42	5.98
Pr	9.94	3.05	3.50	2.07	3.88
Sr	274	645	304	415	362
Nd	36	13.6	15.5	10.9	17.2
Zr	211	80	75	31	154
Hf	6.22	2.40	2.02	1.11	3.83
Sm	5.92	3.21	4.01	3.28	4.29
Eu	0.80	1.08	1.38	1.10	1.44
Gd	4.78	3.19	3.91	3.25	4.56
Tb	0.69	0.52	0.62	0.51	0.77
Dy	3.89	3.17	3.67	3.00	4.76
Y	20.5	14.5	18.2	14.3	23
Ho	0.80	0.64	0.74	0.58	0.97
Er	2.29	1.72	2.01	1.50	2.65
Tm	0.37	0.25	0.29	0.20	0.39
Yb	2.42	1.63	1.80	1.17	2.40
Lu	0.38	0.25	0.27	0.17	0.36
La/Yb	18	6	6	4	5
Nb_N/Th_N	0.09	0.5	0.6	0.8	0.2
Eu*	0.5	1.0	1.1	1.0	1.0
ΣREE	200	62	72	45	83

Notes: Major elements (wt %) were analyzed by XRF and trace elements (ppm) by ICPMS; LOI = loss on ignition; $Eu/Eu^* = EuN/(Sm_N*Gd_N)^{1/2}$; N = chondrite-normalized concentrations, values from Boynton and others (1984).

a 1σ level; mean ages for pooled U/Pb (and Pb/Pb) analyses are quoted with 95 percent confidence interval, and all the results are shown in table 2. Data reduction was carried out using the Isoplot/Ex v. 2.49 program (Ludwig, 2001).

TABLE 2

SIMS zircon U-Pb data of the granitic porphyry and dolerite from the Langshan area

Sample spot	[U] (ppm)	[Th] (ppm)	Th/U	f_{206} (%)	$^{207}Pb/^{206}Pb$	±1σ (%)	$^{207}Pb/^{235}U$	±1σ (%)	$^{206}Pb/^{238}U$	±1σ (%)	$t_{207/206}$ (Ma)	±1σ	$t_{207/235}$ (Ma)	±1σ	$t_{206/238}$ (Ma)	±1σ
DSM04A (N41°05′48″, E107°02′59″)																
1	125	46	0.4	0.32	0.04961	3.38	0.30931	3.70	0.0452	1.50	285.9	4.3	273.6	8.9	285.1	4.2
2	182	73	0.4	0.62	0.05099	3.06	0.31390	3.42	0.0446	1.51	281.9	4.2	277.2	8.3	281.6	4.2
3	220	96	0.4	12.36	0.04451	80.49	0.26911	80.59	0.0438	4.06	278.9	12.9	242.0	190.3	276.6	11.0
4	155	68	0.4	20.13	0.03601	72.45	0.21480	72.53	0.0433	3.27	278.0	11.5	197.6	139.4	273.1	8.8
5	208	102	0.5	66.11	0.03316	200.55	0.18743	200.68	0.0410	7.33	261.4	67.2	174.4	279.4	259.0	18.6
6	195	80	0.4	6.45	0.05113	10.95	0.31146	11.06	0.0442	1.58	278.8	5.0	275.3	27.0	278.7	4.3
7	185	63	0.3	0.13	0.05161	1.83	0.33103	2.38	0.0465	1.53	293.3	4.4	290.3	6.0	293.1	4.4
8	136	59	0.4	0.54	0.05061	3.31	0.30788	3.64	0.0441	1.51	278.7	4.2	272.5	8.7	278.3	4.1
9	193	82	0.4	0.31	0.05018	2.40	0.31941	2.84	0.0462	1.51	291.7	4.4	281.5	7.0	290.9	4.3
10	158	61	0.4	0.25	0.05235	2.42	0.32677	2.84	0.0453	1.50	285.3	4.2	287.1	7.1	285.4	4.2
11	424	332	0.8	0.04	0.05198	1.20	0.32443	1.94	0.0453	1.53	285.4	4.3	285.3	4.8	285.4	4.3
12	293	138	0.5	5.10	0.05132	13.12	0.31892	13.20	0.0451	1.51	284.3	5.0	281.1	32.9	284.2	4.2
13	217	91	0.4	0.77	0.05078	2.85	0.30985	3.22	0.0443	1.50	279.5	4.2	274.1	7.8	279.1	4.1
14	443	376	0.8	0.05	0.05232	1.21	0.31772	1.93	0.0440	1.50	277.7	4.1	280.1	4.7	277.9	4.1
15	111	38	0.3	0.30	0.05241	3.86	0.33513	4.15	0.0464	1.54	292.1	4.5	293.5	10.6	292.2	4.4
16	242	95	0.4	0.07	0.05161	2.62	0.32388	3.02	0.0455	1.50	287.1	4.3	284.9	7.5	286.9	4.2
17	268	139	0.5	0.34	0.05051	3.66	0.30721	3.96	0.0441	1.51	278.7	4.2	272.0	9.5	278.3	4.1
18	407	335	0.8	0.45	0.05396	2.15	0.33644	2.63	0.0452	1.50	284.4	4.2	294.5	6.7	285.1	4.2
19	151	62	0.4	0.25	0.05280	2.30	0.33504	2.75	0.0460	1.50	289.8	4.3	293.4	7.0	290.1	4.3
20	221	151	0.7	21.27	0.03852	45.06	0.22939	45.13	0.0432	2.45	276.6	11.4	209.7	89.3	272.6	6.5
HG22A (N41°45′24.7″, E108°02′45″)																
1	527	155	0.3	0.07	0.05268	1.44	0.33959	2.08	0.0468	1.50	294.4	4.4	296.9	5.4	294.6	4.3
2	598	219	0.4	0.14	0.05188	1.38	0.33586	2.04	0.0470	1.50	295.9	4.4	294.0	5.2	295.8	4.3
3	573	176	0.3	0.12	0.05064	1.92	0.32329	2.46	0.0463	1.55	292.3	4.5	284.4	6.1	291.8	4.4
4	331	113	0.3	0.21	0.05035	2.64	0.32223	3.04	0.0464	1.51	293.1	4.4	283.6	7.5	292.5	4.3
5	781	492	0.6	0.23	0.05189	1.71	0.33793	2.28	0.0472	1.50	297.7	4.4	295.6	5.9	297.5	4.4
6	416	129	0.3	0.03	0.05128	1.85	0.33804	3.55	0.0478	3.03	301.5	9.0	295.7	9.2	301.1	8.9
7	440	201	0.5	0.00	0.14934	0.51	6.79322	1.94	0.3299	1.87	>1200		2084.8	17.3	1837.9	30

Table 2
(continued)

Sample spot	[U] (ppm)	[Th] (ppm)	Th/U	f_{206} (%)	$^{207}Pb/^{206}Pb$	±1σ (%)	$^{207}Pb/^{235}U$	±1σ (%)	$^{206}Pb/^{238}U$	±1σ (%)	$t_{207/206}$ (Ma)	±1σ	$t_{207/235}$ (Ma)	±1σ	$t_{206/238}$ (Ma)	±1σ
HG22A (N41°45′24.7″, E108°02′45″)																
8	522	186	0.4	0.10	0.05189	1.62	0.32596	2.21	0.0456	1.50	287.2	4.3	286.5	5.5	287.2	4.2
9	220	81	0.4	0.07	0.05239	2.63	0.33565	3.03	0.0465	1.50	292.7	4.4	293.9	7.8	292.8	4.3
10	1436	1256	0.9	0.03	0.05205	1.04	0.34429	1.83	0.0480	1.50	302.2	4.5	300.4	4.8	302.0	4.4
11	578	205	0.4	0.05	0.05158	2.43	0.33097	2.86	0.0465	1.50	293.4	4.4	290.3	7.2	293.2	4.3
12	203	73	0.4	0.08	0.05041	2.93	0.31364	3.30	0.0451	1.52	285.1	4.3	277.0	8.0	284.5	4.2
13	1111	642	0.6	0.03	0.05276	1.21	0.33418	1.93	0.0459	1.50	289.3	4.3	292.8	4.9	289.5	4.3
14	349	121	0.3	0.05	0.05339	2.21	0.34054	2.68	0.0463	1.51	291.1	4.4	297.6	6.9	291.5	4.3
15	765	300	0.4	0.05	0.05104	2.29	0.33006	2.74	0.0469	1.50	295.9	4.4	289.6	6.9	295.4	4.3
16	309	130	0.4	0.00	0.05336	2.45	0.33426	2.88	0.0454	1.51	285.9	4.3	292.8	7.4	286.4	4.2
17	425	151	2.2	0.13	0.05224	2.14	0.32973	2.62	0.0458	1.52	288.5	4.3	289.4	6.6	288.6	4.3
18	559	193	0.3	0.03	0.05206	1,14	0.32819	1.89	0.0457	1.50	288.2	4.3	288.2	4.7	288.2	4.2
19	349	119	0.3	0.04	0.05336	2.45	0.32606	2.11	0.0453	1.59	285.8	4.5	286.6	5.3	286.8	4.5
HG11 (N41°30′51″, E107°45′22″)																
~~1~~	~~359~~	~~10~~	~~0.03~~	~~7.83~~	~~0.04542~~	~~16.02~~	~~0.24981~~	~~16.11~~	~~0.0399~~	~~1.62~~	~~253.9~~	~~4.8~~	~~226.4~~	~~33.2~~	~~252.2~~	~~4.0~~
2	353	310	0.88	0.16	0.05147	2.22	0.28381	2.68	0.0400	1.50	252.7	3.8	253.7	6.0	252.8	3.7
3	403	372	0.92	2.30	0.04975	3.37	0.27525	3.69	0.0401	1.50	254.1	3.8	246.9	8.1	253.6	3.7
4	190	153	0.8	0.28	0.04968	4.14	0.27552	4.41	0.0402	1.51	254.8	3.8	247.1	9.7	254.2	3.8
5	466	307	0.66	0.14	0.04971	2.70	0.27601	3.10	0.0403	1.52	255.0	3.9	247.5	6.8	254.5	3.8
6	136	36	0.26	0.00	0.05550	2.86	0.31027	3.23	0.0405	1.51	254.9	3.8	274.4	7.8	256.2	3.8
~~7~~	~~177~~	~~3~~	~~0.02~~	~~5.77~~	~~0.05036~~	~~10.87~~	~~0.28157~~	~~10.97~~	~~0.0405~~	~~1.50~~	~~256.4~~	~~4.4~~	~~251.9~~	~~24.8~~	~~256.2~~	~~3.8~~
8	307	324	1.0	0.25	0.05228	2.04	0.29462	2.54	0.0409	1.51	258.0	3.9	262.2	5.9	258.3	3.8
9	252	5	0.02	0.00	0.05129	1.94	0.28909	2.47	0.0409	1.53	258.3	3.9	257.8	5.7	258.3	3.9
~~10~~	~~129~~	~~4~~	~~0.03~~	~~3.01~~	~~0.04455~~	~~10.48~~	~~0.25142~~	~~10.59~~	~~0.0409~~	~~1.56~~	~~260.8~~	~~4.0~~	~~227.7~~	~~21.8~~	~~258.6~~	~~3.9~~
11	420	3	0.01	0.08	0.05047	1.91	0.28482	2.44	0.0409	1.52	258.9	3.9	254.5	5.5	258.6	3.9
12	123	3	0.02	0.13	0.05223	3.18	0.29572	3.51	0.0411	1.50	259.1	3.9	263.1	8.2	259.4	3.8
13	119	1	0.01	1.28	0.05039	5.55	0.29207	5.76	0.0420	1.52	265.8	4.0	260.2	13.3	265.4	4.0
14	353	17	0.05	0.14	0.04992	1.92	0.28944	2.44	0.0420	1.51	266.1	4.0	258.1	5.6	265.5	3.9

Table 2
(continued)

Sample spot	[U] (ppm)	[Th] (ppm)	Th/U	f_{206} (%)	$^{207}Pb/^{206}Pb$	±1σ (%)	$^{207}Pb/^{235}U$	±1σ (%)	$^{206}Pb/^{238}U$	±1σ (%)	$t_{207/206}$ (Ma)	±1σ	$t_{207/235}$ (Ma)	±1σ	$t_{206/238}$ (Ma)	±1σ
HG11 (N41°30′51″, E107°45′22″)																
15	497	45	0.09	0.00	0.05126	1.40	0.29810	2.05	0.0422	1.50	266.4	4.0	264.9	4.8	266.3	3.9
16	572	40	0.07	0.00	0.05249	1.55	0.30624	2.18	0.0423	1.53	266.9	4.0	271.3	5.2	267.2	4.0
17	1010	113	0.11	0.18	0.05190	1.15	0.30436	1.91	0.0425	1.52	268.4	4.0	269.8	4.5	268.5	4.0
18	86	1	0.01	0.37	0.05073	3.33	0.29845	3.67	0.0427	1.53	269.6	4.1	265.2	8.6	269.3	4.0
19	253	12	0.05	0.10	0.04993	1.80	0.29429	2.35	0.0427	1.51	270.4	4.0	261.9	5.4	269.8	4.0
20	982	18	0.02	0.06	0.05043	1.51	0.29724	2.16	0.0427	1.54	270.3	4.1	264.2	5.0	269.8	4.1
21	208	14	0.07	0.22	0.04907	2.84	0.28946	3.22	0.0428	1.51	270.9	4.1	258.1	7.4	270.0	4.0
22	78	118	1.5	0.00	0.05183	4.22	0.31034	4.49	0.0434	1.51	274.0	4.2	274.4	10.8	274.0	4.1
23	1667	41	0.03	0.02	0.05171	0.97	0.31062	1.79	0.0436	1.50	274.9	4.1	274.7	4.3	274.9	4.0
24	272	5	0.02	0.11	0.05128	1.85	0.31154	2.39	0.0441	1.51	278.1	4.1	275.4	5.8	277.9	4.1

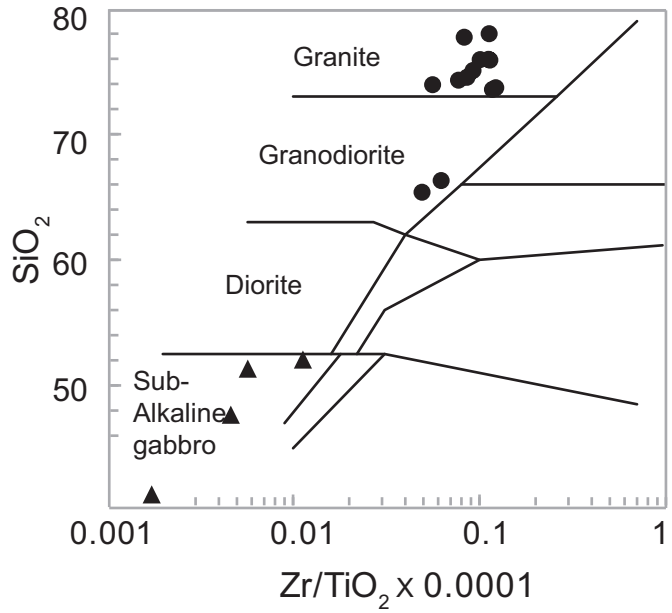

Fig. 4. SiO_2 *vs.* $Zr/TiO_2/10^4$ diagram, based on Winchester and Floyd (1977). Circles are granitic and granodioritic porphyries. Triangles are gabbros and dolerites.

Analytical Results

Whole rock geochemistry.—Field and petrographic investigations reveal that all felsic intrusions have undergone different degrees of metamorphism, whereas mafic rocks experienced no metamorphism or deformation, but some show the effects of weathering. These relations are reflected in the major oxide contents as in felsic intrusive samples with high SiO_2 (65.38-8.00%) and different loss on ignition (LOI) contents (0.62-1.86%), whereas mafic intrusive rocks have low SiO_2 (40.93-50.91%) and loss on ignition (LOI) contents of 0.88 to 3.42 percent (table 1 and fig. 4).

Intrusions DSM04A, B, C in the Lower Zhaertai Group are granitic porphyries with SiO_2 (74.30-75.07%), medium Al_2O_3 (13.35-13.64%), and low contents of TFe_2O_3 (1.29-1.38%), MgO (0.39-0.61%) and K_2O (0.53-0.82%); their REE contents are low <40 ppm and show similar LREE-enriched patterns (La/Yb 6-12). However, DSM04A and B have almost no Eu anomalies (Eu* ~ 1), contrasting with DSM 04C that has a significant negative Eu anomaly (Eu* ~ 0.4) (fig. 5). Granodioritic porphyries (HG01A, B, HG03A, B, HG05A, B, HG22A, B and HG23A, B) are from the Upper Zhaertai Group. HG03A, and B have SiO_2 (65.38-66.31%), medium Al_2O_3 (14.90-15.33%) TFe_2O_3 (3.92-5.07%), and MgO (0. 39-0.61%), and high Na_2O (4.43-4.72%) and K_2O (4.14-3.36%). Their REE contents are relatively high > 240 ppm and show LREE-enriched patterns (La/Yb 53-69) and a negative Eu anomaly (Eu* 0.6-0.7) (fig. 5). The remaining samples are all granitic porphyries with high SiO_2 (73.56-78.00%), and variable contents of Al_2O_3 (11.84-14.22%), TFe_2O_3 (0.36-3.71%), MgO (0.13-0.63%), Na_2O (2.05-4.62%) and K_2O (2.79-4.18%) (fig. 4). The REE contents are between 14 to 204 ppm, and they have LREE-enriched patterns (La/Yb 9-45) and negative Eu anomalies (Eu* 0.4-0.70) (fig. 5).

TYK06, HG04 and HG 08 are gabbros. TYK06 and HG04 have high contents of LOI 2.12 percent and 3.42. HG11 is a very fresh dolerite characterized by low SiO_2

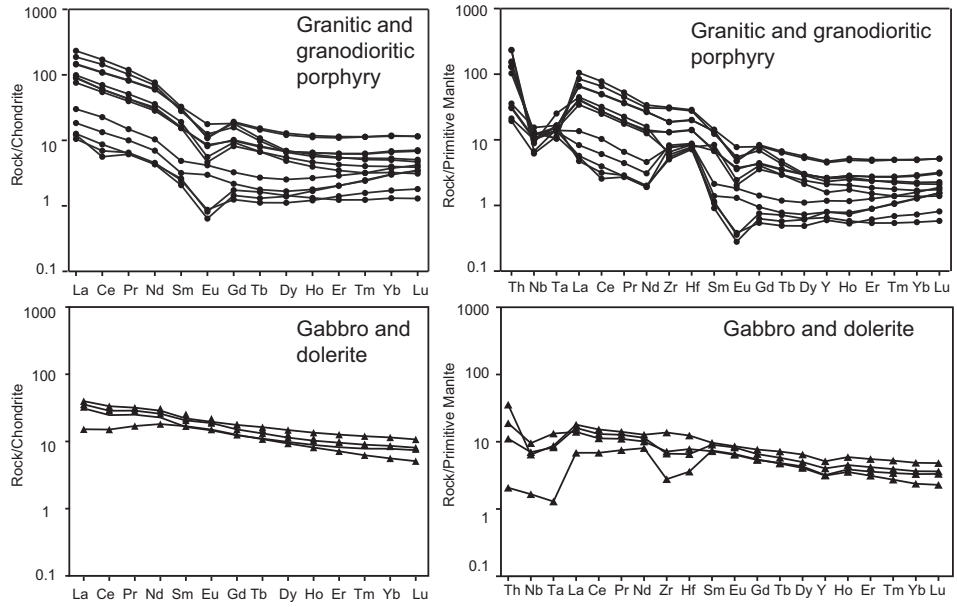

Fig. 5. Chondrite-normalized REE patterns and primitive mantle-normalized trace element diagrams of whole-rock samples of granitic-granodioritic porphyries, gabbros and dolerites from the Langshan area. Chondrite data from Boynton (1984) and Primitive data from Sun and Mcdonough (1989). All samples show negative Nb-Ta anomalies, a subduction-related signature.

42.33 percent and low LOI 0.88; it has high contents of TFe_2O_3 17.99 to 18.55 percent, MgO 9.61 percent, CaO 12.81 percent, and low contents of Na_2O 1.11 and K_2O 0.22. All mafic rocks have coherent REE patterns with La/Yb of 4–6, Σ REE (45-83 ppm), no Eu anomalies (Eu* 1.0-1.1) and negative Nb anomalies (Nb_N/Th_N 0.2-0.8) (fig. 4).

U-Pb analysis of zircon.—Dated samples with separated zircons are granitic porphyries of DSM04A and HG22A and dolerite HG11. The zircons are typically irregular and preserve irregular zonation observed in CL images (fig. 6). Errors of individual analyses are given at 1 s.Measured U-Pb isotopic ratios are presented in table 2. 20 points of 19 zircons from DSM04A were analyzed and 6 rejected on the basis of discordance, probable resetting or high radiogenic Pb. 14 analyses have $^{238}U/^{206}Pb$ ages of 274.4 ± 4.2 Ma to 293.3 ± 4.4 Ma, and weighted mean ages of 284.7 ± 2.1 Ma with MSWD of 1.6 and probability of 0.1. The $^{235}U/^{207}Pb$ and $^{238}U/^{206}Pb$ ratios in table 2 yielded a concordia age of 281 ± 17 Ma with MSWD of 0.87 (fig. 7). Th/U ratios of DSM 04A are between 0.3 and 0.8.

For sample HG22, 19 zircons were analyzed and 1 rejected on the basis of discordance. 18 analyses show $^{238}U/^{206}Pb$ ages of 284.5 ± 4.2 Ma to 302 ± 4.4 Ma, which yielded weighted mean ages of 291.7 ± 2.1 Ma with MSWD of 1.14 and probability of 0.3, whereas the $^{235}U/^{207}Pb$ and $^{238}U/^{206}Pb$ ratios yielded a concordia age of 289.8 ± 9.2 Ma with MSWD of 0.66 (fig. 7); their Th/U ratios are between 0.3 and 0.9.

For sample HG11, 24 zircons were analyzed and three rejected on the basis of discordance. 21 analyses show $^{238}U/^{206}Pb$ ages of 252.8 ± 3.7 Ma to 277.9 ± 4.1 Ma, which yielded weighted mean ages of 263 ± 1.7 Ma with MSWD of 3.9 and probability of 0, whereas the $^{235}U/^{207}Pb$ and $^{238}U/^{206}Pb$ ratios could not yield concordia ages (fig. 7). As shown in figure 6, a group of 9 zircons are clearly younger than others, and the ages of these 9 zircons are quite consistent with each other and yielded a concordia

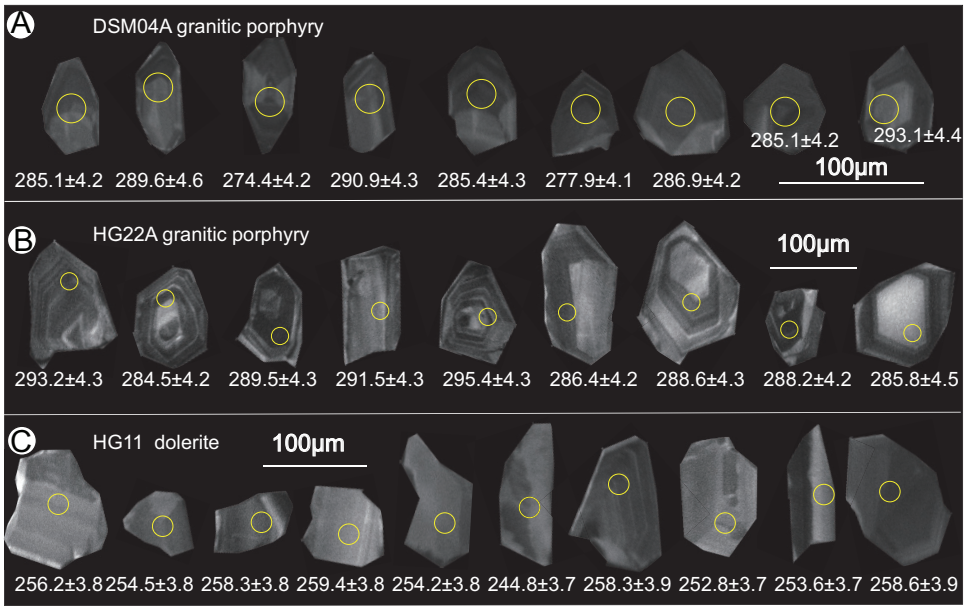

Fig. 6. CL images of representative zircon grains showing the $^{238}U/^{206}Pb$ ages of each analysis. DSM 04A and HG22A are granitic porphyries and HG11 is from dolerites.

ages of 256.2 ± 2.6 Ma, MSWD of 0.42, and weighted mean ages of 256 ± 3.5 Ma with MSWD of 0.48.

DISCUSSION

Petrogenesis and Possible Settings

As mentioned above, all felsic samples underwent low-grade metamorphism, and some mafic rocks experienced weak weathering. As a result, elements like Na, K and fluid mobile elements like Rb, Ba, Sr and Pb cannot be used to indicate possible petrogenetic settings. Many recent studies have indicated that the REE and the high-field strength elements (HFSE, Nb, Zr, Ti, Th), which are considered as immobile during weathering and metamorphic processes, can be mobile in the presence of fluids (Gao and others, 2007; Monecke and others, 2011). There is no evidence that the samples in this study have been hydrothermally altered, and they contain no quartz or calcite veins, and therefore we are able to consider the immobile elements with confidence. In a SiO_2 *vs.* Zr/TiO_2 discrimination diagram (fig. 5), samples intruded in the Lower and Upper Zhaertai Groups plot in the granite field and two intruded in the Upper Zhaertai Group in the granodiorite area. The major oxide contents are consistent with the fact that these are granitic porphyries or granodioritic porphyries that consist predominantly of quartz and feldspar (figs. 2F and 2H) and have a porphyritic texture. On the chondrite-normalized REE diagram (Boynton, 1984), all porphyry samples are LREE-enriched, and show a wide range of Eu anomalies. Two samples from intrusions in the Lower Zhaertai Group contain no or slightly positive anomalies, and one intrusion in the Lower Zhaertai Group and the remaining ten from the Upper Zhaertai Group show negative anomalies. Eu anomalies can be caused by crystallization of plagioclase and by oxygen fugacity (fO_2), because the Eu^{2+}substitutes for Ca^{2+} in the plagioclase (Weill and Drake, 1973). Moreover,

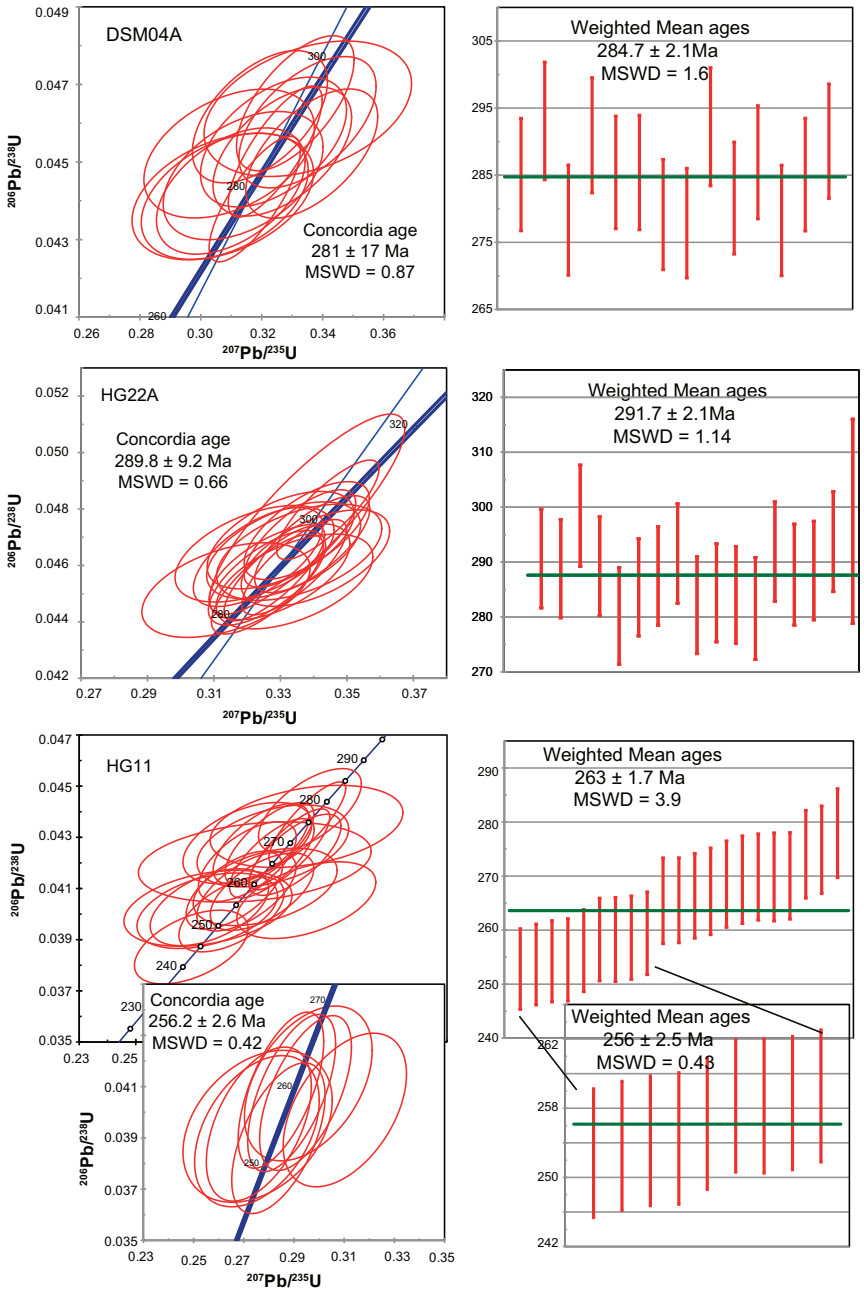

Fig. 7. U-Pb concordia diagrams and weighted mean ages of zircons (sample points shown in fig. 6) from granitic porphyries (DSM 04A and HG22A) and dolerite (HG11).

plagioclase crystallization is related to depth, because it is unstable at a deep level (Martin and Moyen, 2002). Therefore, the Eu anomaly can be an indirect index of the depth of formation of a rock. The contrasting Eu anomalies in the different Langshan samples may be caused by the presence or absence of plagioclase in the residue magma

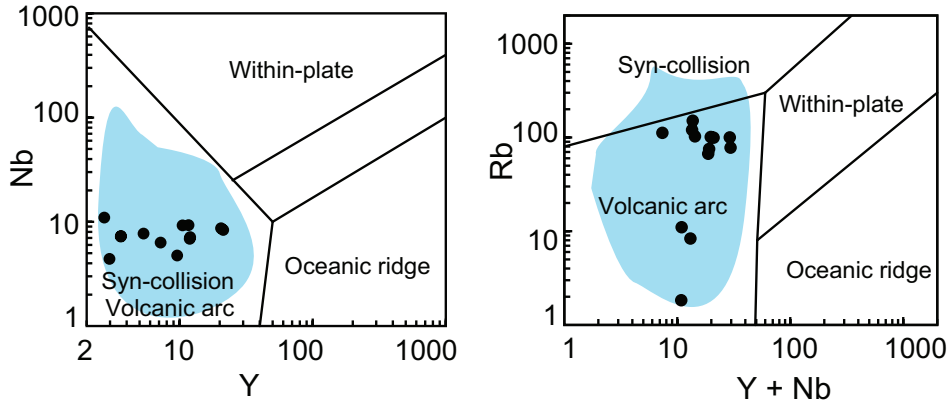

Fig. 8. Tectonic discrimination diagram for granitic rocks based on Pearce and others (1984). The blue areas represent the composition of Permian granites on the northern margin of the North China Craton in the Solonker and Beishan regions in the Central Asian Orogenic belt. Data from Chen and others (2000, 2009); Jahn and others (2004); Wan and others (2009); Jian and others (2010). Black dots are porphyries from this study, showing that they fall in the volcanic arc fields.

source, and are a further indication of different depths in the crust. All porphyry samples show negative Nb anomalies indicating a strong subduction signature (fig. 6). On a tectonic discrimination diagram (Pearce and others, 1984), all samples plot in the volcanic arc or syn-collision granite areas in a Nb *vs.* Y diagram, and in the volcanic arc area in a Rb *vs.* Nb+Y diagram (fig. 8). All our mafic rocks come from shallow level intrusions, so their geochemical signatures are not expected to differ markedly from those of extrusive rocks. The Langhsan mafic samples are all LREE-enriched and have no Eu anomalies; therefore, they might be derived from lithospheric mantle where feldspar is not stable. All the mafic samples are similar to the porphyries in having Nb anomalies, suggesting that the lithosphere had been metasomatized by subduction fluids. However, these geochemical signatures alone cannot be used as definitive proof that these granitic porphyry and doleritic dikes formed in a subduction setting, because lithospheric mantle melts can retain a subduction signature after cessation of subduction, as in the Pliocene magmatic rocks in the Sierra Nevada of California (Putirka and Busby, 2007). The age of the intrusions and their regional geology have also to be considered.

Based on U-Pb zircon analyses, two porphyry samples at different localities yielded very similar weighted mean ages 284.7 ± 2.1 Ma and 291.7 ± 2.1 Ma, which are consistent with concordia ages of 281 ± 17 Ma and 289.8 ± 9.2 Ma within error, respectively (fig. 7). The agreement indicates that the U-Pb system in zircons has not been destroyed or modified since the last thermal event (crystallization or metamorphism). Based on field and thin section observations, the relevant porphyries underwent low greenschist facies metamorphism, the peak temperature of which is *ca.* 450 °C (see for example, Raase, 1974). The closure temperature of zircon is about *ca.* 900 °C (see for example, Corfu and others, 2003), thus greenschist metamorphism cannot change the structure of a zircon and cannot affect the U-Pb system; this is supported by the CL images of zircon in figure 6 and the magmatic Th/U ratio >0.1 (Hoskin and Schaltegger, 2003). Accordingly, the zircon ages in the present study represent the crystallization ages of the granitic porphyries. 21 of our analyzed dolerite samples have no concordia ages, but 9 of the 21 are in good agreement, yielded the concordia age of 256.2 ± 2.6 Ma and the weighted mean age of 256 ± 2.5 Ma. The younger age of 256 Ma may represent the crystallization and emplacement age of the

dolerites, and the older zircons may be xenocrysts entrapped from wall rocks during the magma ascent.

Our ages indicate that all the granitic and mafic rocks crystallized or were intruded in the Permian, indicating that some form of tectonic activity was still in operation in this part of Central Asia (Xiao and others, 2003, 2009). Because a few Archaen rocks and many Proterozoic sediments crop out nearby, the Langshan region was previously considered to be part of the North China Craton (NCC) (Zhao and others, 2001); in other words it was difficult to position the boundary between the NCC and the CAOB in this region. In contrast, in adjacent areas like Solonker east of Langshan, and Alax and Beishan west of Langshan, there are extensive Permian intrusions; extensive studies show that they all share similar geochemical features with our samples, besides the fact that they are also juvenile in origin (Chen and others, 2000, 2009; Jahn and others, 2004; Wan and others, 2009; Jian and others, 2010). Permian ophiolites also occur at Solonker (Jian and others, 2010), Alax (Feng and others, 2013) and Beishan (Mao and others, 2012), and it is reasonable to conclude that they formed in a subduction-related setting before closure of the Paleo-Asian Ocean. The Langshan area is located between Alxa block and Solonker suture. The most striking feature of the Langshan area is the presence of extensive Paleozoic granitoids (Anonymous, 1980, 1981), which were most likely created by reactivation of the North China Craton by oceanic slab subduction beneath the craton in the late Paleozoic (Zhang, S. H. and others, 2006, 2007, 2009). Comparing the ages and geochemistry of our samples with previously published, comparable data from adjacent areas, correlations suggest that our rocks very likely formed in a subduction-related setting. However, our deformed and metamorphosed granitic porphyries are older than the undeformed dolerites, which points to a change in tectonic environment.

Timing of Deformation and Its Significance

In the Langshan area all strata older than Mesozoic are pervasively deformed (fig. 2); the fold axial planes strike E to NE and dip S to SE, and the structural styles of deformation are similar to those elsewhere in the Altaids (Xiao and others, 2003, 2009; Lehmann and others, 2010; Heumann and others, 2012). Large-scale deformation accompanied by regional metamorphism is typical of accretionary orogenic belts, where the time of the youngest deformation can help us to constrain the lower age limits of the accretion and collision, and thus comparison with nearby parts of the southern Altaids will help to contribute to the current debate about when the Altaid orogen terminated.

Field and petrographic observations indicate that the granitic porphyries and their Proterozoic wall rocks are all deformed and metamorphosed (figs. 2E-2H), but their metamorphic grades are different. The granitic porphyries have undergone greenschist facies metamorphism, in contrast to their wall rocks that have amphibolite facies assemblages. Because the wall rocks are much older than the Permian intrusions, they have experienced a more complex history than the Permian intrusions. The Permian porphyries postdate the deformation of the wall rocks, and the porphyry intrusions are characterized by NE-striking and N-vergent orientations and structures. The porphyries were intruded at *ca.* 290 Ma, so the N-vergent deformation must be younger than this age. Considering the fact that the ophiolites to the west at Alxa (Feng and others, 2013) and to the east at Solonker (Jian and others, 2010) have early Permian obduction-accretion ages, a Permian ocean must have been in existence at the time. We propose that the N-vergent deformation of the early Permian granitic porphyries took place during accretion, which was generated by southward subduction of an oceanic slab. The long-lived southward subduction transported huge volumes of water below and into the North China Craton, which substantially altered the composi-

tion of the lithosphere of the northern margin of the craton (Windley and others, 2010). Extensive Paleozoic intrusive igneous rocks (Chen and others, 2000; Wu and others, 2002; Zhang, S. H. and others, 2006, 2007, 2009) and magmatic hydrothermal ore deposits (Wan and others, 2009; Zhang, L. C. and others, 2009) are responses to the reactivation and melting of the lower craton.

In contrast, our late Permian doleritic dikes are undeformed and unmetamorphosed. In general, such undeformed dikes can be generated in a variety of tectonic settings like post-tectonic, extensional, convergent, or transform. However, the Langshan undeformed dikes are *ca.* 50 Ma younger than the deformed porphyries. The late undeformed dolerite dikes did not suffer subsequent penetrative strain and still show subduction-fluid metasomatic fingerprints. Therefore we argue that this part of the North China Craton was an active continental margin, and we are encouraged by the fact that many similar intrusions occur in the American Cordillera and other active continental margins or orogens (Weigand and Ragland, 1970; Hergt and others, 1989; Lapierre and others, 2003; Chiaradia, 2009; Cai and others, 2010). Considering the structural and geochemical data, the late Permian dolerites sets a minimum age for accretionary orogenesis in this area. As described in the Geological Background and Sampling Section, a suite of Mesozoic conglomerates is undeformed and unconformably overlies all the older rocks. These conglomerates are widespread in North China and Inner Mongolia (Anonymous, 1980, 1981). Although, conglomerates, now partly deformed, can be deposited in forearc basins during ongoing subduction, the undeformed Mesozoic conglomerates at Langshan overlie the Precambrian basement of North China and volcanic rocks in Inner Mongolia, which means they covered extensive areas of the North China Craton and Paleozoic island arcs. It is difficult to interpret such widely distributed conglomerates as forearc basin sediments; the only viable explanation is that they are post-orogenic cover sediments deposited after the collision between the North China Craton and surrounding island arcs. The mainly early Jurassic age of the conglomerates (Anonymous, 1981) places a minimum age for the termination of the orogenic activity. The available integrated geological, geochemical and isotopic evidence indicates that the time of termination of the Central Asian orogenesis, in this region at least, can be bracketed between the end-Permian and the early Triassic. Considering the fact that the development of an accretionary orogen is by its nature episodic and that the preserved geological record is incomplete, more studies and more detailed constraints are required to narrow down our time range.

Link Between the East and West Southern Altaids

The Altaids extends EW from E40° in Kyrgyzstan to E135° at the Okhotsk Sea in the Russian Far East (Sengör and others, 1993) (fig. 1 inset). In spite of reservations by Kröner and others (2014), large quantities of juvenile material were added to the crust during accretion of the Altaids (Sengör and others, 1993; Jahn and others, 2004; Kröner and others, 2007; Windley and others, 2007; Wilhem and others, 2012). The general consensus today is that the Altaid orogenic collage terminated in the south (Xiao and others, 2003).

In the Tianshan orogen in Kyrgyzstan double (or two-sided)-subduction took place in the Late Paleozoic (Hegner and others, 2010; Rolland and others, 2013). However, in the orogen that strikes eastwards to the Chinese Tianshan, evidence of northward subduction in the late Paleozoic is clearly indicated by a huge accretionary complex to the south of the Tianshan arc and north of the Tarim passive margin, but there is no evidence that the northern Tarim margin was active during the Paleozoic (Xiao and others, 2008, 2013; Ao and others, 2010). Although Charvet and others (2007) proposed that double subduction had been operative in the South Tianshan orogen, many lines of evidence suggest that the western part of the Tarim Craton remained passive since the early Paleozoic, and that the South Tianshan assemblages

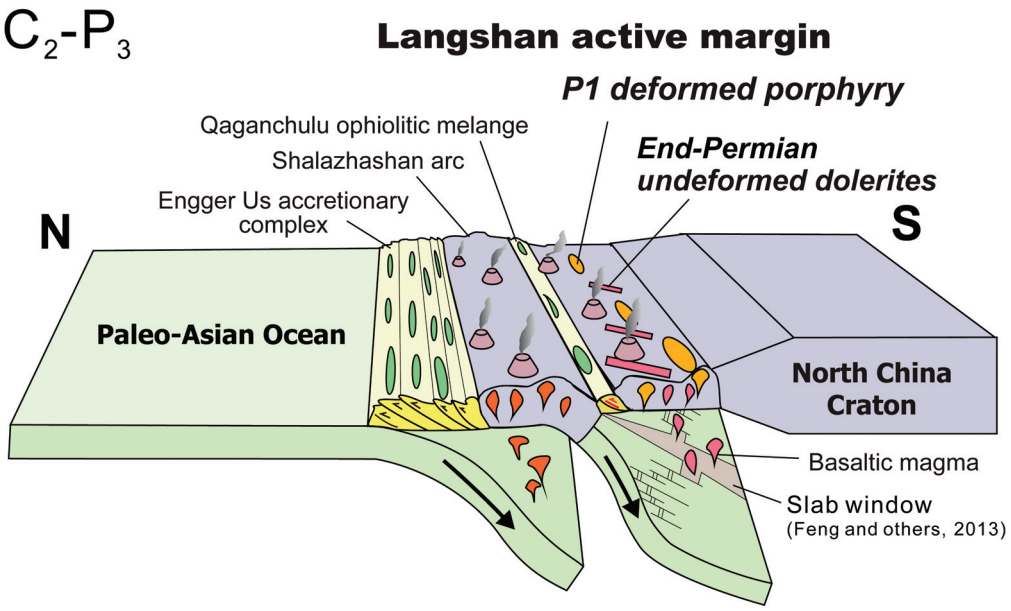

Fig. 9. Plate tectonic model illustrating the distribution of key rocks and assemblages on the northern active continental margin of the North China Craton in the Langshan region during the Late Carboniferous to Permian (modified after Feng and others, 2013).

were part of an accretionary complex related to the northward subduction of the Tarim Craton (Xiao and others, 2013).

Farther east, double subduction in the late Permian to early Triassic in the Beishan region (Xiao and others, 2010b; Guo and others, 2012; Mao and others, 2012) was associated with strong deformation that gave rise to mega-fold superimposition and km-scale interference patterns (Zhang, J., and Cunningham, 2012) interpreted as an expression of the terminal tectonic activity of the southern Altaids (Tian and others, 2013). To the east of the Beishan orogen, a major desert covers the Alxa and Langshan areas where similar mega-fold patterns may be present (Zhang, S. H. and others, 2007; Feng and others, 2013). Farther north in southern Mongolia complicated re-deformation took place in the late Paleozoic-early Mesozoic (Guy and others, 2014). Feng and others (2013) identified a Late Carboniferous to Late Permian accretionary complex in the Alxa region, where limited outcrops suggest that the deformation was vergent to the north.

The Langshan belt is to the east of Alxa. As discussed above, an Andean-type continental magmatic arc that was built on the margin of the North China Craton in the late Paleozoic indicates southward subduction beneath the craton. To the east of the Langshan belt is the Solonker suture, where extensive geological and geochemical studies have demonstrated that double subduction took place in the Late Paleozoic (see for example, Xiao and others, 2003; Miao and others, 2008; Jian and others, 2010), and this is confirmed by a recent seismic reflection profile (Zhang and others, 2014).

As reviewed above, the whole Southern Altaids is characterized by remarkably contemporaneous orogenic timing in the Late Paleozoic, but tectonic styles were not uniform, that is double-direction subduction and/or northward subduction in different regions. Because the Archean and Proterozoic rocks are scattered and because of

the extensive Mesozoic and Cenozoic cover in the Langshan area, its Paleozoic history has not been fully evaluated. From this study we conclude that there was a Permian Andean-type arc in the Langshan area (fig. 9); hence the late Paleozoic boundary between the North China Craton and the Altaids must be re-positioned.

The orogenic style is very similar to that in the Beishan and Solonker orogens. These parts of the Southern Altaids were characterized by south-dipping subduction in the Permian, in contrast to the coeval northward subduction in the Chinese Tianshan. The now-defunct, long-lived single subduction model proposed by Sengör and others (1993) cannot explain the contrasting structures and geological evolution of the Southern Altaids. There is now indubitable evidence for more than one independent subduction system in the late Paleozoic, as one would expect in a complex archipelago.

CONCLUSIONS

Based on our field and petrographic observations, and geochemical and geochronological studies of granitic and granodioritic porphyries, gabbro and dolerite dikes intruded into the Proterozoic Zhaertai Group in the Langshan area, we draw the following conclusions:

(1) The granitic and granodioritic porphyries are characterized by high SiO_2 (65.38-78.00%), low TFe_2O_3 (1.29-5.07%) and MgO (0.13-0.63%) and variable K_2O (0.53-4.14%) and Na_2O (2.05-4.62%). All samples have enriched LREE (La/Yb 1.1-6.8) and negative Nb anomalies (Nb_N/Th_N0.09-0.48), but variable Eu anomalies (Eu* $<$0.7 or $\sim$1). The gabbros and dolerites have 42.33 to 52.03 percent SiO_2. All mafic samples have similar La/Yb ratios of 4 to 6 and negative Nb anomaly (Nb_N/Th_N) ratios of 0.2 to 0.8. These geochemical features indicate a heterogeneous source in a subduction-related setting.

(2) Two dated samples yielded $^{238}U/^{206}Pb$ weighted mean ages of 284.7 $\pm$ 2.1 Ma with MSWD of 1.6 and 291.7 $\pm$ 2.1 Ma with MSWD of 1.14; these two ages are comparable with $^{235}U/^{207}Pb$ and $^{238}U/^{206}Pb$ concordia ages of 281 $\pm$ 17 Ma with MSWD of 0.87 and 289.8 $\pm$ 9.2 Ma with MSWD of 0.66. Supported by the CL images and Th/U ratios $>$ 0.1 these early Permian ages are consistent with and reflect the times of crystallization. Based on the intrusive-time-deformation relationships between the porphyries and sediments, the igneous rocks were emplaced before the deformation. The time of crystallization of the dolerites was between the concordia age of 256.2 $\pm$ 2.6 Ma with MSWD of 0.44 and the weighted mean age of 256 $\pm$ 2.5 Ma with MSWD of 0.45.

(3) Our geochemical and chronological data integrated with earlier studies indicate that the Langshan belt was an active continental margin arc built on the northern margin of the North China Craton by southward subduction in the Late Paleozoic. The changes in timing and orogenic style in the Permian in the Langshan region are very similar to those at Beishan and Alxa in the west and Solonker in the east, but they are different from those in the Chinese Tianshan. The contrasting, but coeval, orogenic styles favor an archipelago model of subduction-accretion-collision.

ACKNOWLEDGMENTS

We dedicate this study to Professor Bor-ming Jahn who has long been working on the tectonics of the Central Asian Orogenic Belt. Many thanks are due to Guochao Zuo and Richard Glen for helpful discussions. We appreciate the critical comments of John Wakabayashi, Bin Chen, and Kuo-Lung Wang, which greatly improved the paper. This study was financially supported by the Chinese National Basic Research 973 Program (2012CB416604, 2014CB448000), the National Natural Science Foundation of China (41390445, 41230207, 41390441, 41190075, and 41272107), the One Hundred Talent Program B of the Chinese Academy of Sciences, the Chinese National Basic Research 973 Program (2007CB411307), and the National 305 Projects (2011BAB06B01 and

2007BAB25B04). B. Wan wishes to thank the Visiting Scholar Program of the Chinese Academy of Sciences. This is a contribution to IGCP 592.

References

Alekseev, D. V., Aristov, V. A., and Degtyarev, K. E., 2007, The age and tectonic setting of volcanic and cherty sequences in the ophiolite complex of the Atbashe Ridge (Southern Tien Shan): Doklady Earth Sciences, v. 413, n. 2, p. 380–383, http://dx.doi.org/10.1134/S1028334X07030130

Allen, M. B., Windley, B. F., and Zhang, C., 1993, Palaeozoic collisional tectonics and magmatism of the Chinese Tien Shan, Central Asia: Tectonophysics, v. 220, n. 1–4, p. 89–115, http://dx.doi.org/10.1016/0040-1951(93)90225-9

Anonymous, 1980, 1:200000 Geological and Metallogenic map and Explanation note of Hailisu Sheet: The First Geological Survey Team of Inner Mongolia.

——— 1981, 1:200000 Geological map and Explanation note of Sandaoqiao Sheet, Linhe Sheet, Wulatehouqi Sheet: The First Geological Survey Team of Inner Mongolia.

Ao, S. J., Xiao, W. J., Han, C. M., Mao, Q. G., and Zhang, J. E., 2010, Geochronology and geochemistry of Early Permian mafic-ultramafic complexes in the Beishan area, Xinjiang, NW China: Implications for late Paleozoic tectonic evolution of the southern Altaids: Gondwana Research, v. 18, n. 2–3, p. 466–478, http://dx.doi.org/10.1016/j.gr.2010.01.004

Badarch, G., Cunningham, W. D., and Windley, B. F., 2002, A new terrane subdivision for Mongolia: implications for the Phanerozoic crustal growth of Central Asia: Journal of Asian Earth Sciences, v. 21, n. 1, p. 87–110, http://dx.doi.org/10.1016/S1367-9120(02)00017-2

Boynton, W. V., 1984, Geochemistry of the rare earth elements: Meteorite studies, *in* Henderson, P., editor, Rare Earth Element Geochemistry: Amsterdam, Elsevier, p. 63–114.

Cai, K., Sun, M., Yuan, C., Zhao, G., Xiao, W., Long, X., and Wu, F., 2010, Geochronological and geochemical study of mafic dykes from the northwest Chinese Altai: Implications for petrogenesis and tectonic evolution: Gondwana Research, v. 18, n. 4, p. 638–652, http://dx.doi.org/10.1016/j.gr.2010.02.010

Charvet, J., Shu, L., and Laurent-Charvet, S., 2007, Paleozoic structural and geodynamic evolution of eastern Tianshan (NW China): welding of the Tarim and Junggar plates: Episodes, v. 30, p. 162–185.

Chen, B., Jahn, B. M., Wilde, S. A., and Xu, B., 2000, Two contrasting Paleozoic magmatic belts in northern Inner Mongolia, China: petrogenesis and tectonic implications: Tectonophysics, v. 328, n. 1–2, p. 157–182, http://dx.doi.org/10.1016/S0040-1951(00)00182-7

Chen, B., Jahn, B. M., and Tian, W., 2009, Evolution of the Solonker suture zone: Constraints from zircon U–Pb ages, Hf isotopic ratios and whole-rock Nd–Sr isotope compositions of subduction- and collision-related magmas and forearc sediments: Journal of Asian Earth Sciences, v. 34, n. 3, p. 245–257, http://dx.doi.org/10.1016/j.jseaes.2008.05.007

Chiaradia, M., 2009, Adakite-like magmas from fractional crystallization and melting-assimilation of mafic lower crust (Eocene Macuchi arc, Western Cordillera, Ecuador): Chemical Geology, v. 265, n. 3–4, p. 468–487, http://dx.doi.org/10.1016/j.chemgeo.2009.05.014

Coleman, R. G., 1989, Continental growth of northwest China: Tectonics, v. 8, n. 2, p. 621–635, http://dx.doi.org/10.1029/TC008i003p00621

Corfu, F., Hanchar, J. M., Hoskin, P. W. O., and Kinny, P., 2003, Atlas of zircon textures: Reviews in Mineralogy and Geochemistry, v. 53, p. 469–500, http://dx.doi.org/10.2113/0530469

Cunningham, W. D., Windley, B. F., Dorjnamjaa, D., Badamgarov, G., and Saandar, M., 1996, A structural transect across the Mongolian Western Altai: Active transpressional mountain building in central Asia: Tectonics, v. 15, n. 1, p. 142–156, http://dx.doi.org/10.1029/95TC02354

Darby, B. J., and Ritts, B. D., 2007, Mesozoic structural architecture of the Lang Shan, North-Central China: Intraplate contraction, extension, and synorogenic sedimentation: Journal of Structural Geology, v. 29, n. 12, p. 2006–2016, http://dx.doi.org/10.1016/j.jsg.2007.06.011

Dewey, J. F., 1969, Continental margins: A model for conversion of Atlantic type to Andean type: Earth and Planetary Science Letters, v. 6, n. 3, p. 189–197, http://dx.doi.org/10.1016/0012-821X(69)90089-2

Ding, T. P., and Jiang, S. Y., 2000, Stable Isotope study of the Langshan polymetallic mineral district, Inner Mongolia, China: Resource Geology, v. 50, n. 1, p. 25–38, http://dx.doi.org/10.1111/j.1751-3928.2000.tb00053.x

Dobretsov, N. L., Berzin, N. A., and Buslov, M. M., 1995, Opening and tectonic evolution of the Paleo-Asian Ocean: International Geology Review, v. 37, n. 4, p. 335–360, http://dx.doi.org/10.1080/00206819509465407

Feng, J., Xiao, W. J., Windley, B., Han, C., Wan, B., Zhang, J. E., Ao, S., Zhang, Z., and Lin, L., 2013, Field geology, geochronology and geochemistry of mafic-ultramafic rocks from Alxa, China: Implications for Late Permian accretionary tectonics in the southern Altaids: Journal of Asian Earth Sciences, v. 78, p. 114–142, http://dx.doi.org/10.1016/j.jseaes.2013.01.020

Gao, J., 1997, The discovery of the eclogites and its tectonic implications, southwest Tianshan: Chinese Science Bulletin, v. 42, p. 737–740.

Gao, J., John, T., Klemd, R., and Xiong, X., 2007, Mobilization of Ti-Nb-Ta during subduction: Evidence from rutile-bearing dehydration segregations and veins hosted in eclogite, Tianshan, NW China: Geochimica et Cosmochimica Acta, v. 71, n. 20, p. 4974–4996, http://dx.doi.org/10.1016/j.gca.2007.07.027

Guo, Q., Xiao, W. J., Windley, B. F., Mao, Q., Han, C., Qu, J., Ao, S., Li, J., Song, D., and Yong, Y., 2012, Provenance and tectonic settings of Permian turbidites from the Beishan Mountains, NW China:

Implications for the Late Paleozoic accretionary tectonics of the southern Altaids: Journal of Asian Earth Sciences, v. 49, p. 54–68, http://dx.doi.org/10.1016/j.jseaes.2011.03.013

Guy, A., Schulmann, K., Clauer, N., Hasalova, P., Seltmann, R., Armstrong, R., Lexa, O., and Benedicto, A., 2014, Late Palaeozoic-Mesozoic tectonic evolution of the Trans-Altai and South Gobi Zones in southern Mongolia based on structural and geochronological data: Gondwana Research, v. 25, n. 1, p. 309–337, http://dx.doi.org/10.1016/j.gr.2013.03.014

Hegner, E., Klemd, R., Kröner, A., Corsini, M., Alexeiev, D. V., Iaccheri, L. M., Zack, T., Dulski, P., Xia, X., and Windley, B. F., 2010, Mineral ages and P–T conditions of Late Paleozoic high-pressure eclogite and provenance of mélange sediments from Atbashi in the South Tianshan orogen of Kyrgyzstan: American Journal of Science, v. 310, n. 9, p. 916–950, http://dx.doi.org/10.2475/09.2010.07

Hergt, J. M., Chappell, B. W., McCulloch, M. T., McDougall, I., and Chivas, A. R., 1989, Geochemical and isotopic constraints on the origin of the Jurassic dolerites of Tasmania: Journal of Petrology, v. 30, n. 4, p. 841–883, http://dx.doi.org/10.1093/petrology/30.4.841

Heumann, M. J., Johnson, C. L., Webb, L. E., Taylor, J. P., Jalbaa, U., and Minjin, C., 2012, Paleogeographic reconstruction of a late Paleozoic arc collision zone, southern Mongolia: Geological Society of America Bulletin, v. 124, n. 9–10,p. 1514–1534, http://dx.doi.org/10.1130/B30510.1

Hoskin, P. W. O., and Schaltegger, U., 2003, The composition of zircon and igneous and metamorphic petrogenesis: Reviews in Mineralogy and Geochemistry, v. 53, p. 27–62, http://dx.doi.org/10.2113/0530027

Hsü, K. J., 2003, Role of ophiolites in archipelago model of orogenesis: Geological Society of America Special Papers, v. 373, p. 159–171, http://dx.doi.org/10.1130/0-8137-2373-6.159

Hsü, K. J., Wang, Q. C., Li, L., and Hao, J., 1991, Geologic evolution of the Neimonides—a working hypothesis: Eclogae Geologicae Helvetiae, v. 84, n. 1, p. 1–31.

Jahn, B. M., Capdevila, R., Liu, D., Vernon, A., and Badarch, G., 2004, Sources of Phanerozoic granitoids in the transect Bayanhongor-Ulaan Baatar, Mongolia: geochemical and Nd isotopic evidence, and implications for Phanerozoic crustal growth: Journal of Asian Earth Sciences, v. 23, n. 5, p. 629–653, http://dx.doi.org/10.1016/S1367-9120(03)00125-1

Jian, P., Liu, D., Kröner, A., Windley, B. F., Shi, Y., Zhang, W., Zhang, F., Miao, L., Zhang, L., and Tomurhuu, D., 2010, Evolution of a Permian intraoceanic arc-trench system in the Solonker suture zone, Central Asian Orogenic Belt, China and Mongolia: Lithos, v. 118, n. 1–2, p. 169–190, http://dx.doi.org/10.1016/j.lithos.2010.04.014

Khain, E. V., Bibikova, E. V., Kröner, A., Zhuravlev, D. Z., Sklyarov, E. V., Fedotova, A. A., and Kravchenko-Berezhnoy, I. R., 2002, The most ancient ophiolite of the Central Asian fold belt: U-Pb and Pb-Pb zircon ages for the Dunzhugur Complex, Eastern Sayan, Siberia, and geodynamic implications: Earth and Planetary Science Letters, v. 199, n. 3–4, p. 311–325, http://dx.doi.org/10.1016/S0012-821X(02)00587-3

Kröner, A., Windley, B. F., Badarch, G., Tomurtogoo, O., Hegner, E., Jahn, B. M., Gruschka, S., Khain, E. V., Demoux, A., and Wingate, M. T. D., 2007, Accretionary growth and crust-formation in the central Asian Orogenic Belt and comparison with the Arabian-Nubian shield, *in* Hatcher, R. D., Carlson, M. P., McBride, J. H., and Catalán, M., editors, 4-D Framework of Continental Crust: Geological Society of America Memoir 200, p. 181–209, http://dx.doi.org/10.1130/2007.1200(11)

Kröner, A., Kovach, V., Belousova, E., Hegner, E., Armstrong, R., Dolgopolova, A., Seltmann, R., Alexeiev, D. V., Hoffmann, J. E., Wong, J., Sun, M., Cai, K., Wang, T., Tong, Y., Wilde, S. A., Degtyarev, K. E., and Rytsk, E., 2014, Reassessment of continental growth during the accretionary history of the Central Asian Orogenic Belt: Gondwana Research, v. 25, n. 1, p. 103–125, http://dx.doi.org/10.1016/j.gr.2012.12.023

Kusky, T. M., Windley, B. F., Safonova, I., Wakita, K., Wakabayashi, J., Polat, A., and Santosh, M., 2013, Recognition of ocean plate stratigraphy in accretionary orogens through Earth history: A record of 3.8 billion years of sea floor spreading, subduction, and accretion: Gondwana Research, v. 24, n. 2, p. 501–547, http://dx.doi.org/10.1016/j.gr.2013.01.004

Lapierre, H., Bosch, D., Tardy, M., and Struik, L. C., 2003, Late Paleozoic and Triassic plume-derived magmas in the Canadian Cordillera played a key role in continental crust growth: Chemical Geology, v. 201, n. 1–2, p. 55–89, http://dx.doi.org/10.1016/S0009-2541(03)00224-9

Lehmann, J., Schulmann, K., Lexa, O., Corsini, M., Kröner, A., Stipská, P., Tomurhuu, D., and Otgonbator, D., 2010, Structural constraints on the evolution of the Central Asian Orogenic Belt in SW Mongolia: American Journal of Science, v. 310, n. 7, p. 575–628, http://dx.doi.org/10.2475/07.2010.02

Li, Q. L., Chen, F., Guo, J.-H., Li, X.-H., Yang, Y.-H., and Siebel, W., 2007, Zircon ages and Nd–Hf isotopic composition of the Zhaertai Group (Inner Mongolia): Evidence for early Proterozoic evolution of the northern North China Craton: Journal of Asian Earth Sciences, v. 30, n. 3–4, p. 573–590, http://dx.doi.org/10.1016/j.jseaes.2007.01.006

Li, Q. L., Li, X., Liu, Y., Tang, G., Yang, J., and Zhu, W., 2010, Precise U-Pb and Pb-Pb dating of Phanerozoic baddeleyite by SIMS with oxygen flooding technique: Journal of Analytical Atomic Spectrometry, v. 25, p. 1107–1113, http://dx.doi.org/10.1039/b923444f

Li, X., Liu, Y., Li, Q., Li, Guo, C., and Chamberlain, K. R., 2009, Precise determination of Phanerozoic zircon Pb/Pb age by multicollector SIMS without external standardization: Geochemistry, Geophysics, Geosystems, v. 10, n. 4, p. Q04010, http://dx.doi.org/10.1029/2009GC002400

Lu, S. N., Yang, C. L., Li, H. K., and Li, H. M., 2002, A group of rifting events in the terminal Paleoproterozoic in the North China Craton: Gondwana Research, v. 5, n. 1, p. 123–131, http://dx.doi.org/10.1016/S1342-937X(05)70896-0

Ludwig, K. R., 2001, Isoplot/Ex, rev. 2.49: A Geochronological Toolkit for Microsoft Excel, v. 1a: Berkeley, Berkeley Geochronological Center, 55 p.

Mao, Q., Xiao, W. J., Windley, B. F., Han, C., Qu, J., Ao, S., Zhang, J. e., and Guo, Q., 2012, The Liuyuan complex in the Beishan, NW China: a Carboniferous–Permian ophiolitic fore-arc sliver in the southern Altaids: Geological Magazine, v. 149, n. 3, p. 483–506, http://dx.doi.org/10.1017/S0016756811000811

Martin, H., and Moyen, J.-F., 2002, Secular changes in tonalite-trondhjemite-granodiorite composition as markers of the progressive cooling of Earth: Geology, v. 30, n. 4, p. 319–322, http://dx.doi.org/10.1130/0091-7613(2002)030⟨0319:SCITTG⟩2.0.CO;2

Miao, L., Fan, W., Liu, D., Zhang, F., Shi, Y., and Guo, F., 2008, Geochronology and geochemistry of the Hegenshan ophiolitic complex: Implications for late-stage tectonic evolution of the Inner Mongolia-Daxinganling Orogenic Belt, China: Journal of Asian Earth Sciences, v. 32, n. 5–6, p. 348–370, http://dx.doi.org/10.1016/j.jseaes.2007.11.005

Monecke, T., Kempe, U., Trinkler, M., Thomas, R., Dulski, P., and Wagner, T., 2011, Unusual rare earth element fractionation in a tin-bearing magmatic-hydrothermal system: Geology, v. 39, n. 4, p. 295–298, http://dx.doi.org/10.1130/G31659.1

Pearce, J. A., Harris, N. B. W., and Tindle, A. G., 1984, Trace-element discrimination diagrams for the tectonic interpretation of granitic rocks: Journal of Petrology, v. 25, n. 4, p. 956–983, http://dx.doi.org/10.1093/petrology/25.4.956

Peng, R., and Zhai, Y., 2004, Hydrothermal mineralization on the Mesoproterozoic passive continental margins of China: A case study of the Langshan-Zha'ertaishan Belt, Inner Mongolia, China: Acta Geologica Sinica-English Edition, v. 78, p. 534–547.

Peng, R., Zhai, Y., Han, X., Wang, Z., Wang, J., and Liu, J., 2007, Sinsedimentry volcanic activities in the cracking process of the Mesoproterozoic aulacogen of passive continental margin in Langshan-Zhaertai area, Inner Mongolia, and its indicating significance: Acta Petrologica Sinica, v. 23, p. 1007–1017 (in Chinese with English Abstract).

Peng, R., Zhai, Y., Wang, J., Chen, X., Liu, Q., Lv, J., Shi, Y., Wang, G., Li, S., Wang, L., Ma, Y., and Zhang, P., 2010, Discovery of Neoproterozoic acid volcanic rock in the south-western section of Langshan, Inner Mongolia: Chinese Science Bulletin, v. 55, p. 2611.

Putirka, K., and Busby, C. J., 2007, The tectonic significance of high-K_2O volcanism in the Sierra Nevada, California: Geology, v. 35, n. 10, p. 923–926, http://dx.doi.org/10.1130/G23914A.1

Raase, P., 1974, Al and Ti contents of hornblende, indicators of pressure and temperature of regional metamorphism: Contributions to Mineralogy and Petrology, v. 45, n. 3, p. 231–236, http://dx.doi.org/10.1007/BF00383440

Rolland, Y., Alexeiev, D. V., Kröner, A., Corsini, M., Loury, C., and Monie, P., 2013, Late Palaeozoic to Mesozoic kinematic history of the Talas-Ferghana strike-slip fault (Kyrgyz West Tianshan) as revealed by $^{40}Ar/^{39}Ar$ dating of syn-kinematic white mica: Journal of Asian Earth Sciences, v. 67–68, p. 76–92, http://dx.doi.org/10.1016/j.jseaes.2013.02.012

Sengör, A. M. C., 1991, Timing of orogenic events: a persistent geological controversy, *in* Müller, D. W., McKenzie, J. A., and Weissert, H., editors, Controversies in Modern Geology: Evolution of Geological Theories in Sedimentology, Earth History and Tectonics: London, Academic Press, p. 405–473.

Sengör, A. M. C., and Natal'in, B. A., 1996, Paleotectonics of Asia: fragments of a synthesis, *in* Yin, A., and Harrison, M., editors, The Tectonic Evolution of Asia: Cambridge, Cambridge University Press, p. 486–640.

Sengör, A. M. C., Natal'in, B. A., and Burtman, V. S., 1993, Evolution of the Altaid tectonic collage and Palaeozoic crustal growth in Eurasia: Nature, v. 364, p. 299–307, http://dx.doi.org/10.1038/364299a0

Stacey, J. S., and Kramers, J. D., 1975, Approximation of terrestrial lead isotope evolution by a two-stage model: Earth and Planetary Science Letters, v. 26, n. 2, p. 207–221, http://dx.doi.org/10.1016/0012-821X(75)90088-6

Sun, S. S., and McDonough, W. F., 1989, Chemical and isotopic systematics of ocean basins: implications for mantle composition and processes, *in* Saunders, A. D., and Norry, M. J., editors, Magmatism in the Ocean Basins: Geological Society, London, Special Publications, v. 42, p. 313–345, http://dx.doi.org/10.1144/GSL.SP.1989.042.01.19

Tang, K. D., 1990, Tectonic development of Palaeozoic foldbelts at the north margin of the Sino-Korean craton: Tectonics, v. 9, n. 2, p. 249–260, http://dx.doi.org/10.1029/TC009i002p00249

Tian, Z., Xiao, W. J., Shan, Y., Windley, B. F., Han, C., Zhang, J. E., and Song, D., 2013, Mega-fold interference patterns in the Beishan orogen (NW China) created by change in plate configuration during Permo-Triassic termination of the Altaids: Journal of Structural Geology, v. 52, p. 119–135, http://dx.doi.org/10.1016/j.jsg.2013.03.016

Wan, B., Hegner, E., Zhang, L., Rocholl, A., Chen, Z., Wu, H., and Chen, F., 2009, Rb-Sr geochronology of chalcopyrite from the Chehugou porphyry Mo-Cu deposit (Northeast China) and geochemical constraints on the origin of hosting granites: Economic Geology, v. 104, n. 3, p. 351–363, http://dx.doi.org/10.2113/gsecongeo.104.3.351

Weigand, P. W., and Ragland, P. C., 1970, Geochemistry of Mesozoic dolerite dikes from eastern North America: Contributions to Mineralogy and Petrology, v. 29, n. 3, p. 195–214, http://dx.doi.org/10.1007/BF00373305

Weill, D. F., and Drake, M. J., 1973, Europium anomaly in plagioclase feldspar: Experimental results and semiquantitative model: Science, v. 180, n. 4090, p. 1059–1060, http://dx.doi.org/10.1126/science.180.4090.1059

Wiedenbeck, M., Allé, P., Corfu, F., Griffin, W. L., Meier, M., Oberli, F., Quadt, A. V., Roddick, J. C., and Spiegel, W., 1995, Three natural zircon standards for U-Th-Pb, Lu-Hf, trace element and REE analyses: Geostandards Newsletter, v. 19, n. 1, p. 1–23, http://dx.doi.org/10.1111/j.1751-908X.1995.tb00147.x

Wilhem, C., Windley, B. F., and Stampfli, G. M., 2012, The Altaids of Central Asia: A tectonic and evolutionary innovative review: Earth-Science Reviews, v. 113, n. 3–4, p. 303–341, http://dx.doi.org/10.1016/j.earscirev.2012.04.001

Winchester, J. A., and Floyd, P. A., 1977, Geochemical discrimination of different magma series and their differentiation products using immobile elements: Chemical Geology, v. 20, p. 325–343, http://dx.doi.org/10.1016/0009-2541(77)90057-2

Windley, B. F., Kröner, A., Guo, J. H., Qu, G. S., Li, Y. Y., and Zhang, C., 2002, Neoproterozoic to Paleozoic geology of the Altai Orogen, NW China: New zircon age data and tectonic evolution: The Journal of Geology, v. 110, n. 6, p. 719–737, http://dx.doi.org/10.1086/342866

Windley, B. F., Alexeiev, D., Xiao, W. J., Kröner, A., and Badarch, G., 2007, Tectonic models for accretion of the Central Asian Orogenic Belt: Journal of the Geological Society, London, v. 164, n. 1, p. 31–47, http://dx.doi.org/10.1144/0016-76492006-022

Windley, B. F., Maruyama, S., and Xiao, W. J., 2010, Delamination/thinning of sub-continental lithospheric mantle under Eastern China: The role of water and multiple subduction: American Journal of Science, v. 310, n. 10, p. 1250–1293, http://dx.doi.org/10.2475/10.2010.03

Wu, F. Y., Sun, D. Y., Li, H. M., Jahn, B.-M., and Wilde, S. A., 2002, A-type granites in northeastern China: age and geochemical constraints on their petrogenesis: Chemical Geology, v. 187, n. 12, p. 143–173, http://dx.doi.org/10.1016/S0009-2541(02)00018-9

Xiao, W. J., Windley, B. F., Hao, J., and Zhai, M. G., 2003, Accretion leading to collision and the Permian Solonker suture, Inner Mongolia, China: Termination of the central Asian orogenic belt: Tectonics, v. 22, n. 6, 1069, http://dx.doi.org/10.1029/2002TC001484

Xiao, W. J., Han, C., Yuan, C., Sun, M., Lin, S., Chen, H., Li, Z., Li, J., and Sun, S., 2008, Middle Cambrian to Permian subduction-related accretionary orogenesis of Northern Xinjiang, NW China: Implications for the tectonic evolution of central Asia: Journal of Asian Earth Sciences, v. 32, n. 2–4, p. 102–117, http://dx.doi.org/10.1016/j.jseaes.2007.10.008

Xiao, W. J., Windley, B. F., Huang, B. C., Han, C. M., Yuan, C., Chen, H. L., Sun, M., Sun, S., and Li, J. L., 2009, End-Permian to mid-Triassic termination of the accretionary processes of the southern Altaids: implications for the geodynamic evolution, Phanerozoic continental growth, and metallogeny of Central Asia: International Journal of Earth Sciences, v. 98, n. 6, p. 1189–1217, http://dx.doi.org/10.1007/s00531-008-0407-z

Xiao, W. J., Huang, B., Han, C., Sun, S., and Li, J., 2010a, A review of the western part of the Altaids: A key to understanding the architecture of accretionary orogens: Gondwana Research, v. 18, n. 2–3, p. 253–273, http://dx.doi.org/10.1016/j.gr.2010.01.007

Xiao, W. J., Mao, Q. G., Windley, B. F., Han, C. M., Qu, J. F., Zhang, J. E., Ao, S. J., Guo, Q. Q., Cleven, N. R., Lin, S. F., Shan, Y. H., and Li, J. L., 2010b, Paleozoic multiple accretionary and collisional processes of the Beishan orogenic collage: American Journal of Science, v. 310, n. 10, p. 1553–1594, http://dx.doi.org/10.2475/10.2010.12

Xiao, W. J., Windley, B. F., Allen, M. B., and Han, C., 2013, Paleozoic multiple accretionary and collisional tectonics of the Chinese Tianshan orogenic collage: Gondwana Research, v. 23, n. 4, p. 1316–1341, http://dx.doi.org/10.1016/j.gr.2012.01.012

Zhai, M., and Liu, W., 2003, Palaeoproterozoic tectonic history of the North China Craton: a review: Precambrian Research, v. 122, n. 1–4, p. 183–199, http://dx.doi.org/10.1016/S0301-9268(02)00211-5

Zhang, J., and Cunningham, W. D., 2012, Kilometer-scale refolded folds caused by strike-slip reversal and intraplate shortening in the Beishan region, China: Tectonics, v. 31, n. 3, TC3009, http://dx.doi.org/10.1029/2011TC003050

Zhang, J., Li, J., Xiao, W., Wang, Y., and Qi, W., 2013, Kinematics and geochronology of multistage ductile deformation along the eastern Alxa block, NW China: New constraints on the relationship between the North China Plate and the Alxa block: Journal of Structural Geology, v. 57, p. 38–57, http://dx.doi.org/10.1016/j.jsg.2013.10.002

Zhang, L. C., Wu, H., Wan, B., and Chen, Z., 2009a, Ages and geodynamic settings of Xilamulun Mo-Cu metallogenic belt in the northern part of the North China Craton: Gondwana Research, v. 16, n. 2, p. 243–254, http://dx.doi.org/10.1016/j.gr.2009.04.005

Zhang, S. H., Zhao, Y., and Song, B., 2006, Hornblende thermobarometry of the Carboniferous granitoids from the Inner Mongolia paleo-uplift: implications for the tectonic evolution of the northern margin of North China block: Mineralogy and Petrology, v. 87, n. 1–2, p. 123–141, http://dx.doi.org/10.1007/s00710-005-0116-2

Zhang, S. H., Zhao, Y., Song, B., Yang, Z., Hu, J., and Wu, H., 2007, Carboniferous granitic plutons from the northern margin of the North China block: implications for a late Palaeozoic active continental margin: Journal of the Geological Society, London, v. 164, n. 2, p. 451–463, http://dx.doi.org/10.1144/0016-76492005-190

Zhang, S. H., Zhao, Y., Song, B., Hu, J.-M., Liu, S.-W., Yang, Y.-H., Chen, F.-K., Liu, X.-M., and Liu, J., 2009b, Contrasting Late Carboniferous and Late Permian–Middle Triassic intrusive suites from the northern margin of the North China Craton: Geochronology, petrogenesis, and tectonic implications: Geological Society of America Bulletin, v. 121, n. 1–2, p. 181–200, http://dx.doi.org/10.1130/B26157.1

Zhang, S. H., Gao, R., Li, H. Y., Hou, H. S., Hu, H. C., Li, Q. S., Yang, K., Li, C., Li, W. H., Zhang, J. S., Yang, T. S., Keller, G. R., and Liu, M., 2014, Crustal structure revealed from a deep seismic reflection profile across the Solonker suture zone of the Central Asian Orogenic Belt, northern China: An integrated interpretation: Tectonophysics, v. 612–613, p. 26–39, http://dx.doi.org/10.1016/j.tecto.2013.11.035

Zhao, G., Wilde, S. A., Cawood, P. A., and Sun, M., 2001, Archean blocks and their boundaries in the North China Craton: lithological, geochemical, structural and *P-T* path constraints and tectonic evolution: Precambrian Research, v. 107, n. 1–2, p. 45–73, http://dx.doi.org/10.1016/S0301-9268(00)00154-6

Zonenshain, L. P., Kuzmin, M. I., and Natapov, L. M., 1990, Geology of the USSR: A Plate-Tectonic Synthesis: Washington D.C., American Geophysical Union, Geodynamic Series, v. 12, p. 242.